PHILOSOPHICAL TRANSACTIONS OF THE ROYAL SOCIETY B BIOLOGICAL SCIENCES

The Aerodynamics of Hovering Insect Flight. III. Kinematics

C. P. Ellington

Phil. Trans. R. Soc. Lond. B 1984 **305**, 41-78
doi: 10.1098/rstb.1984.0051

Phil. Trans. R. Soc. Lond. B **305**, 41–78 (1984)

Printed in Great Britain

THE AERODYNAMICS OF HOVERING INSECT FLIGHT. III. KINEMATICS

By C. P. ELLINGTON

Department of Zoology, University of Cambridge, Downing Street, Cambridge CB2 3EJ, U.K.

(*Communicated by Sir James Lighthill, F.R.S.* – *Received* 28 *March* 1983)

[Plates 1–7]

CONTENTS

Insects in free flight were filmed at 5000 frames per second to determine the motion of their wings and bodies. General comments are offered on flight behaviour and manoeuvrability. Changes in the tilt of the stroke plane with respect to the horizontal provides kinematic control of manoeuvres, analogous to the type of control used for helicopters.

A projection analysis technique is described that solves for the orientation of the animal with respect to a camera-based coordinate system, giving full kinematic details for the longitudinal wing and body axes from single-view films. The technique can be applied to all types of flight where the wing motions are bilaterally symmetrical: forward, backward and hovering flight, as well as properly banked turns. An analysis of the errors of the technique is presented, and shows that the reconstructed angles for wing position should be accurate to within 1–2° in general. Although measurement of the angles of attack was not possible, visual estimations are given.

Only 11 film sequences show flight velocities and accelerations that are small enough for the flight to be considered as 'hovering'. Two sequences are presented for a hover-fly using an inclined stroke plane, and nine sequences of hovering with a horizontal stroke plane by another hover-fly, two crane-flies, a drone-fly, a ladybird beetle, a honey bee, and two bumble bees. In general, oscillations in the body position from its mean motion are within measurement error, about 1–2% of the wing length. The amplitudes of oscillation for the body angle are only a few degrees, but the phase relation of this oscillation to the wingbeat cycle could be determined for a few sequences. The phase indicates that the pitching moments governing the oscillations result from the wing lift at the ends of the wingbeat, and not from the wing drag or inertial forces. The mean pitching moment of the wings, which determines the mean body angle, is controlled by shifting the centre of lift over the cycle by changing the mean positional angle of the flapping wings.

Deviations of the wing tip path from the stroke plane are never large, and no consistent pattern could be found for the wing paths of different insects; indeed, variations in the path were even observed for individual insects. The wing motion is not greatly different from simple harmonic motion, but does show a general trend towards higher accelerations and decelerations at either end of the wingbeat, with constant velocities during the middle of half-strokes. Root mean square and cube root mean cube angular velocities are on average about 4 and 9% lower than simple harmonic motion. Angles of attack are nearly constant during the middle of half-strokes, typically 35° at a position 70% along the wing length. The wing is twisted along its length, with angles of attack at the wing base some 10–20° greater than at the tip.

The wings rotate through about 110° at either end of the wingbeat during 10–20% of the cycle period. The mean velocity of the wing edges during rotation is similar to the mean flapping velocity of the wing tip and greater than the flapping velocity for more proximal wing regions, which indicates that vortex shedding during rotation is comparable with that during flapping. The wings tend to rotate as a flat plate during the first half of rotation, which ends just before, or at, the end of the half-stroke. The hover-fly using an inclined stroke plane provides a notable exception to this general pattern: pronation is delayed and overlaps the beginning of the downstroke. The wing profile flexes along a more or less localized longitudinal axis during the second half

PHILOSOPHICAL TRANSACTIONS OF THE ROYAL SOCIETY B BIOLOGICAL SCIENCES

of rotation, generating the 'flip' profile postulated by Weis-Fogh for the hover-flies. This profile occurs to some extent for all of the insects, and is not exceptionally pronounced for the hover-fly. By the end of rotation the wings are nearly flat again, although a slight camber can sometimes be seen.

Weis-Fogh showed that beneficial aerodynamic interference can result when the left and right wings come into contact during rotation at the end of the wingbeat. His 'fling' mechanism creates the circulation required for wing lift on the subsequent half-stroke, and can be seen on my films of the Large Cabbage White butterfly, a plume moth, and the Mediterranean flour moth. However, their wings 'peel' apart like two pieces of paper being separated, rather than fling open rigidly about the trailing edges. A 'partial fling' was found for some insects, with the wings touching only along posterior wing areas. A 'near fling' with the wings separated by a fraction of the chord was also observed for many insects. There is a continuous spectrum for the separation distance between the wings, in fact, and the separation can vary for a given insect during different manoeuvres. It is suggested that these variants on Weis-Fogh's fling mechanism also generate circulation for wing lift, although less effectively than a complete fling, and that changes in the separation distance may provide a fine control over the amount of lift produced.

1. Introduction

A quantitative description of the wing motion, or kinematics, during flapping flight is necessary for mechanical and aerodynamic analyses. Relatively few such descriptions can be found in the literature, though, and most theoretical studies assume a sinusoidal motion of the wings by default. With but a single exception, the most accurate and complete studies of wing kinematics have dealt with insects tethered in wind tunnels (Weis-Fogh 1956; Jensen 1956; Nachtigall 1966; Zarnack 1972). Although the artificial constraints imposed by tethering are obviously undesirable, the method greatly simplifies the tasks of photography and kinematic analysis. A wind tunnel was also used by Bilo (1971, 1972) for his detailed analysis of the wing movements of the house sparrow *Passer domesticus*, but the bird was induced to remain in position by behavioural training rather than by mechanical constraint. This free flight under controlled conditions provides the best experimental basis for observations, and has now been applied to some insects: David (1978, 1979, 1982) has used optomotor responses to 'tether' *Drosophila* in a wind tunnel while studying certain aspects of their flight mechanics.

The method of investigation most suitable for this study is that of Magnan (1934), which uses high-speed cinematography to observe animals during free flight in still air. Films of hovering, slow flight and a variety of turning and climbing manoeuvres may be obtained, illustrating the kinematic control of flapping flight. A large filming area is required because of the freedom allowed to the animal. I have found that a horizontal coverage about eight times the wing length is needed to study the flight pattern; if a greater magnification is used, then one cannot determine whether the animal is in steady flight or subject to the acceleration forces of a manoeuvre. A multiple-view single camera system should not be used, therefore, because the film images would then be too small for accurate measurements.

Detailed kinematics have been derived from single-view films by using either a mechanical reconstruction of the film image (Magnan 1934), which is a tedious and inaccurate procedure, or else the projection of the wing length when the orientation of the insect with respect to the camera is known (Weis-Fogh 1956; Jensen 1956). For animals in free flight, the wing motion within a camera-based coordinate system can be determined by the projected wing length, but

the orientation of this movement with respect to the animal is apparent in only three special cases: a front/back, side, or top/bottom view. The last case is unsatisfactory, however, because important information about the vertical component of the flight path is lost. Except for trained birds and bats, most animals appear regrettably ignorant of the merits of the other two cases, and the experimenter is usually left with an unknown direction of view. A projection analysis technique that finds this direction for single-view films is presented here, enabling full kinematic details to be determined for the longitudinal wing and body axes. The analysis assumes that the wings do not bend significantly along their longitudinal axes, which is approximately true for most insects and hummingbirds, and that the flight path lies in the plane of symmetry of the animal. Unfortunately, a quantitative analysis of the angle of attack remains intractable.

The kinematics during free flight have been measured for most of the insects of paper II. Only those sequences that can be considered as 'hovering' are presented in detail here, but some general comments are offered for the other sequences.

2. Materials and methods

The collection, care and identification of the insects has already been described in paper II. I also attempted to study the Mediterranean flour moth *Ephestia kuehniella* Zeller (Pyralidae), which is reared in the Departmental Field Station, but this proved unsuccessful. Films of identified individuals could not be obtained, and the longitudinal wing bending was too great for the assumption of the analysis technique.

2.1. *Filming*

Single insects were filmed inside a flight chamber, which measured 0.2 m square and 0.25 m high. The front and rear panels of the chamber were cut from clear glass and frosted opal glass, respectively, and slid upwards in grooves for access to the insect. The remaining construction was in Perspex. Reference points for the film analysis were provided by two rods, 0.5 mm in diameter, that descended from the chamber top into the upper margin of the filming area. Only a few insects flew spontaneously within the chamber under normal room lighting and temperature (21 °C), and so it was usually necessary to 'persuade' them to perform. Increasing the chamber temperature and illumination by switching on the photographic lights for a brief period often proved sufficient, but tapping the chamber was sometimes required in addition to this. Tactile 'stimulation' with a small brush was used as a last resort on the most reluctant insects. Not surprisingly, almost all insects would fly under these provocations. Although the treatment may have elicited extreme behavioural responses, the resulting kinematics should still be aerodynamically valid. Two insects, *Coccinella* and *Chrysopa*, proved incapable of sustained flight within the confines of the chamber, and were filmed during take-off. When placed on a vertical Perspex rod about 7 mm in diameter, they would climb to its top and, after a brief hesitation and inspection, would almost invariably take off.

An automatic detector circuit switched on the camera and lights when the insect flew through the centre of the filming area. A single light beam and photodetector monitored the trigger point, as shown in figure 1*a*, and this proved much easier to set up and adjust than the usual crossed-beam detector system. A fibre optic light source was focused on the trigger point, as was a photodiode on the side of the chamber. An insect passing through the trigger point caused some of the light beam to be reflected towards the photodiode, resulting in an increased signal

from it. This signal was gated by a Schmitt trigger and then used to operate the switching relays. When a take-off was filmed, the detector was positioned such that it was triggered by the wing movements preparatory to take-off.

The general filming set-up is illustrated in figure 1*b*. The glass front of the chamber faced a Hyspeed 16 mm cine camera (John Hadland (P.I.), U.K.), which was operated at 5000 frames per second: a timing light within the camera housing marked the film at 1 ms intervals. A zoom lens provided focal lengths between 60 and 85 mm, and apertures typically ranged from $f/8$

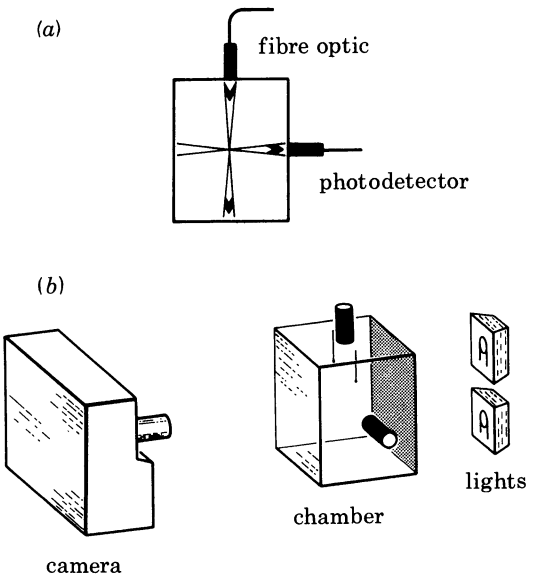

FIGURE 1. (*a*) The reflected-beam detector for the flight chamber. (*b*) The filming set-up. See text for explanation.

to $f/11$. Two 1 kW Q.I. cine lights illuminated the opal glass from behind, producing a silhouette film image of the insect. Room lighting and reflexions of the cine lights within the chamber showed some surface detail on the silhouette. Attempts at front-lighting were abandoned because of intense reflexions from the wings during some parts of the wingbeat cycle.

Ilford Pan F cine film was used in the camera, and was developed for maximum film speed and contrast in Ilford P.Q. Developer (1:9) for about 6 min at 27 °C. The negatives were used for quantitative film analysis, but qualitative notes were taken from positive copies made on a 16 mm continuous contact printer designed and built by G. G. Runnalls and D. J. Tyler in this department.

2.2. *Film analysis*

A film analysis system was constructed around a 16 mm projection head (Model M-16C, Vanguard Instrument Corporation, Long Island, New York) and a PDP 8/I computer equipped with a four channel, 10 bit analogue-to-digital converter (a.d.c.). The projection head was mounted on a framework containing a front-surface mirror, which reflected the projected frame onto the back of a viewing screen. The magnification of this system was approximately × 42. A cursor on the front of the screen was connected to two ten-turn potentiometers, and produced analogue voltages for the a.d.c. proportional to the rectangular coordinates of a point on the screen. The 10 bit a.d.c. limited the resolution to about 1.3% of the projected wing length over the entire frame: the position of the body with respect to one reference point was measured

to this accuracy. The gain of the analogue amplifiers was doubled for measurements of wing and body coordinates with respect to a wing base, restricting coverage to one-quarter of the frame area with an increase in accuracy to 0.6 % of the wing length. A third analogue channel, operated by push-buttons, was used to command the a.d.c. and identify the pair of coordinates entering the PDP 8/I memory. All computer programs were written in a special laboratory version of FOCAL – one of the standard interactive PDP 8/I languages – developed by J. H. Davidson in the Department of Applied Mathematics and Theoretical Physics.

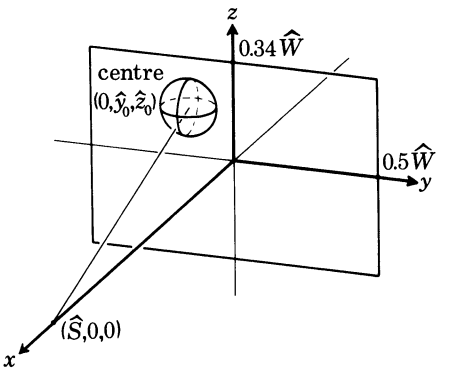

FIGURE 2. Object field for the filming geometry. The object plane is given by yz, the optical axis lies on the x axis, and the optical centre of the lens is at $\hat{S}$. The object sphere has unit radius. The filming area for a standard 16 mm frame is bounded by $y = \pm 0.5\hat{W}$ and $z = \pm 0.34\hat{W}$, where $\hat{W}$ is the ratio of horizontal coverage to wing length. All linear dimensions are expressed in wing lengths.

Geometrical analysis of the films mainly involves reconstructing the spatial angles of an object wing using its projected length in a two-dimensional film image. A spherical surface describing all possible positions of a wing tip, centred at the corresponding wing base, provides an abstract representation of the object (figure 2). In this system, only three parameters govern the filming geometry: the horizontal coverage $\hat{W}$, the distance $\hat{S}$ from the object plane to the optical centre of the lens, and the position $(O, \hat{y}_0, \hat{z}_0)$ of the centre of the sphere. The linear dimensions denoted by a 'hat' are non-dimensional and expressed in wing lengths. $\hat{S}$ may be calculated from simple lens theory as

$$\hat{S} = (f/R)\,(1 + 1/M), \tag{1}$$

where f is the focal length, R is the wing length, and M is the magnification (= image wing length/R). $\hat{W}$ is typically 8 for the films, and the minimum value of $\hat{S}$ is 40 wing lengths.

The geometrical effects of perspective have been neglected in the film analysis by invoking two approximations: (i) all projection rays from the object are parallel to the ray passing through the centre of the sphere, and (ii) these rays are parallel to the horizontal xy plane. The image is therefore interpreted as an orthographic projection of an object sphere that is free to rotate about its vertical axis. The errors introduced by these approximations (and by other sources) are investigated in the Appendix and shown to be negligible. For $\hat{S} = 40$ and $\hat{W} = 8$, the reconstructed angles will be less than 1–2° in error over the entire filming area, and the assumed horizontal plane will deviate less than 2.5° from the true horizontal. Equations to calculate the maximum errors for different values of $\hat{S}$ and $\hat{W}$ are presented in the Appendix.

The perspective error analysis also indicates that the reference wing length should be measured from the frame showing the maximum projected length, and not estimated from the

optical magnification. Even so, measurement inaccuracies and a finite filming speed can produce large errors ($\pm 8°$) in the calculated wing position for that frame. This is unavoidable in a projection analysis, unfortunately, and the data for such frames must be considered as unreliable. For other frames during the wingbeat, the reconstructed angles will still be accurate to within ± 1–$2°$ in general.

2.3. *Kinematic analysis*

Only one wing base can usually be seen when filming an insect from a single camera view; the opposite base may be hidden behind the body. The three-dimensional motion of one wing can thus be determined with respect to the *filming coordinate system* by using its projected length, but this motion cannot be related immediately to the orientation of the insect body. The coordinates of the opposite wing tip (with hidden base) may be used to define the geometrical transformation, however, when the wing motions are *bilaterally symmetrical*. The analysis is therefore restricted to flight patterns where the body travels in the plane of symmetry of the animal: all types of forward, backward and hovering flight can be treated, as well as properly banked turns. A large filming area is required for the observer to verify that the selected flight sequence is truly symmetrical, and it also proves essential in choosing sequences that show approximately *steady* flight.

One wing base could always be identified because of the faint surface detail recorded on the silhouette image, and the corresponding wing tip was usually visible even when in front of the body. Although this information eliminates the reversed-image ambiguity of the silhouette, it was not used in the analysis procedure: the wing with a visible base was always defined as the left wing to simplify calculations, and the silhouette interpretation consistent with this was selected by the computer program.

2.3.1. *Filming coordinate system*

The first stage of the procedure involved digitizing seven points on each frame of the sequence and storing the yz coordinates in the computer. Two of these points, the timing mark and the reference point, are not of direct interest to the kinematic analysis. The remaining points are shown in figure 3*a*: P_1, the visible wing base; P_2, the corresponding wing tip; P_3, the opposite wing tip; P_4, anterior end of the body axis; P_5, posterior end of the body axis. The coordinates of P_1 were measured with respect to its position in the initial frame of the sequence, the reference point being used to correct for frame misalignment in the projector and camera. The coordinates of P_2–P_5 were specified with the origin of the x, y, z axes translated to the visible wing base, as in figure 3*a*. After all frames had been digitized, the maximum projected wing length R' was determined and used to normalize the coordinates. The x coordinate of the wing tip P_2 was then calculated as

$$x_2 = \pm (1 - y_2^2 - z_2^2)^{\frac{1}{2}}; \qquad (2)$$

the sign must be determined by the observer, remembering that the wing is considered to be the left one.

2.3.2. *Coordinate system fixed in the body*

(*a*) *Coordinate transformation*. The wing and body positions must now be transformed to another coordinate system (x', y', z') fixed in the body, which is illustrated in figure 3*b*. The origin is again situated at the wing base, and the x' axis is defined as horizontal. The y' axis passes through the wing bases and is therefore parallel to the line joining the wing tips according

to the symmetrical assumption. This axis is not necessarily horizontal, allowing for the case where the insect is rolled or banked through some angle η about the x' axis. The coordinate transformation is

$$x' = \lambda_1 x + \mu_1 y, \tag{3}$$

$$y' = \lambda_2 x + \mu_2 y + \nu_2 z, \tag{4}$$

$$z' = \lambda_3 x + \mu_3 y + \nu_3 z, \tag{5}$$

where (λ, μ, ν) are the direction cosines of the x', y', z' axes with respect to the x, y, z axes. Because the x' axis is horizontal, $\nu_1 = 0$.

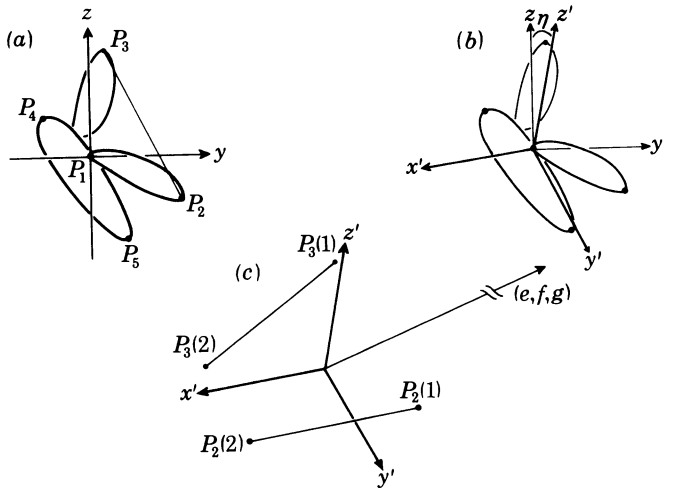

FIGURE 3. (a) Points on each frame used in the kinematic analysis, with the filming coordinate system translated to the visible wing base. (b) The coordinate system fixed in the body, with the x' axis horizontal and the y' axis passing through the wing bases. (c) Constructing a line (e,f,g) parallel to the plane of symmetry, by adding the lines that connect the wing tips at two moments in the cycle.

There are several methods whereby the direction cosines can be found by using the symmetry condition, but I shall only describe the one that I have found to be most accurate. The procedure basically involves finding the direction of the y' axis by using the symmetry condition and data from two frames, then defining the x' axis by the intersection of the plane perpendicular to the y' axis and the horizontal plane $y = 0$, and finally solving for the z' axis which forms an orthogonal set. The direction cosines were calculated for each wingbeat.

The line joining the two wing tips is parallel to the y' axis in individual frames, and its direction in the (x, y, z) system may be written as

$$(a, 1, c) = \left(\frac{x_2 - x_3}{y_2 - y_3}, 1, \frac{z_2 - z_3}{y_2 - y_3}\right). \tag{6}$$

The direction number $\dot{c}$ is simply the slope of the line joining the wing tips on the two-dimensional film image (figure 3a): a mean value $\bar{c}$ was calculated for the wingbeat by weighting the values in each frame by the square of the projected line length, which should be proportional to its variance. The direction of the y' axis cannot be determined completely, however, because the x_3 coordinate of the opposite wing tip is unknown.

This direction can be found from a line perpendicular to the y' axis. Such a line may be defined by the wing tip positions in two frames of the wingbeat, as illustrated in figure 3c. Lines are

first constructed between corresponding wing tips in frames 1 and 2, but the x direction of the line joining the opposite wing tips is unknown. The two lines are equal in length when the wing motions are symmetrical, however, and so this direction can be calculated,

$$x_3(1)-x_3(2) = \pm\{[x_2(1)-x_2(2)]^2+[y_2(1)-y_2(2)]^2+[z_2(1)-z_2(2)]^2 - [y_3(1)-y_3(2)]^2-[z_3(1)-z_3(2)]^2\}^{\frac{1}{2}}, \quad (7)$$

and the sign must be determined by the observer. Vector addition of the two lines then results in a direction (e, f, g) that is parallel to the plane of symmetry,

$$e = x_2(1)-x_2(2)+x_3(1)-x_3(2), \quad (8)$$

$$f = y_2(1)-y_2(2)+y_3(1)-y_3(2), \quad (9)$$

$$g = z_2(1)-z_2(2)+z_3(1)-z_3(2). \quad (10)$$

Because this line is perpendicular to the y' axis, the unknown direction a in equation (6) can now be solved:

$$a = (-f-g\bar{c})/e. \quad (11)$$

The direction of the y' axis can be determined with considerable accuracy using this method. Vector subtraction of the connecting lines would yield this direction immediately, but the resultant would be short and its direction prone to error. By adding the lines and choosing two frames at either end of the wingbeat, a long vector which is very accurate in direction is obtained, and the estimate of a is greatly improved. The results for several combinations of frames at either end of the wingbeat were averaged to produce a mean value $\bar{a}$ for the analysis.

Once the directions of the y' axis are found, those for the x' and z' axes can be calculated as outlined above. The direction cosines are then given by

$$(\lambda_1, \mu_1, \nu_1) = \left(\pm\frac{1}{d_1}, \mp\frac{\bar{a}}{d_1}, 0\right), \quad (12)$$

$$(\lambda_2, \mu_2, \nu_2) = \left(\pm\frac{\bar{a}}{d_2}, \pm\frac{1}{d_2}, \pm\frac{\bar{c}}{d_2}\right), \quad (13)$$

$$(\lambda_3, \mu_3, \nu_3) = \left(-\frac{\bar{a}\bar{c}}{d_1 d_2}, -\frac{\bar{c}}{d_1 d_2}, \frac{\bar{a}+1}{d_1 d_2}\right), \quad (14)$$

where the normalizing factors are

$$d_1 = (1+\bar{a}^2+\bar{c}^2)^{\frac{1}{2}}, \quad (15)$$

$$d_2 = (1+\bar{a}^2)^{\frac{1}{2}}. \quad (16)$$

The choice of signs for the direction cosines of the x' and y' axes is easily made. When the insect is facing the right side of the frame, towards $y > 0$, μ_1 must be positive and λ_2 negative; these signs are reversed when the insect is facing towards the left.

Once the direction cosines have been determined for the wingbeat, the coordinates of the wing tip P_2 can be transformed to the (x', y', z') system by using equations (3)–(5). The coordinates of the body points P_1, P_4 and P_5 cannot be transformed, however, until appropriate values have been calculated for x. For the purposes of the kinematic analysis, we may simply take the projection of these points onto the $x'z'$ plane by rays that are parallel to the x axis. The x coordinate for P_1, P_4 and P_5 can then be calculated by

$$x = (-\mu_2 y-\nu_2 z)/\lambda_2, \quad (17)$$

and the coordinates can now be transformed.

PHILOSOPHICAL TRANSACTIONS OF THE ROYAL SOCIETY B BIOLOGICAL SCIENCES

(*b*) *Kinematic parameters of the body*. The kinematic parameters for the body are illustrated in figure 4*a*. The mean flight velocity $\hat{V}$ is expressed non-dimensionally as the number of wing lengths travelled per wingbeat, and is positive in forward flight. The angle between the mean flight path and the horizontal x' axis is denoted by ξ, which is positive when the insect is climbing. These two parameters were calculated by a linear regression of z_1' on x_1' for the transformed wing base coordinates. The angle χ between the longitudinal body axis and the horizontal x' axis is readily calculated from (x_4', z_4') and (x_5', z_5'). Values of $\hat{V}$, ξ and χ are unreliable for approximately front/back camera views, however, because the projected x' coordinates of the body points are then very sensitive to small measurement errors. The roll angle η, shown in figure 3*b*, is equal to $\cos^{-1}(v_3)$; it is given a negative sign when the left wing is below horizontal.

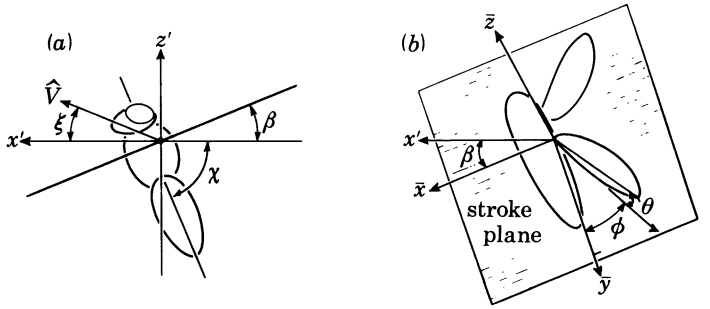

FIGURE 4. (*a*) The kinematic parameters relative to the coordinate system fixed in the body. (*b*) The kinematic parameters for the wings relative to the coordinate system fixed in the stroke plane. See text for explanation.

The wing motion is approximately confined to a plane during flapping flight, the *stroke plane*. This plane is tilted at an angle β to the horizontal x' axis, and passes through the wing bases. I have defined β by the slope of the linear regression line of z' on x' for the wing tip P_2.

2.3.3. *Coordinate system fixed in the stroke plane*

(*a*) *Coordinate transformation*. A third coordinate system, based on the stroke plane, was constructed for the description of the wing kinematics. The new axes $(\bar{x}, \bar{y}, \bar{z})$ are obtained by rotating the old ones (x', y', z') about the y' axis through the angle β:

$$\bar{x} = x' \cos\beta - z' \sin\beta, \tag{18}$$

$$\bar{y} = y', \tag{19}$$

$$\bar{z} = x' \sin\beta + z' \cos\beta. \tag{20}$$

This system is fixed in the stroke plane, as shown in figure 4*b*, and is a logical choice for the wing motion.

(*b*) *Kinematic parameters of the wings*. The wing position is described by spherical coordinates (ϕ, θ) for this system based in the stroke plane, where

$$\phi = \tan^{-1}(-\bar{x}_2/\bar{y}_2), \tag{21}$$

$$\theta = \tan^{-1}[\bar{z}_2/(\bar{x}_2^2 + \bar{y}_2^2)^{\frac{1}{2}}]. \tag{22}$$

The positional angle ϕ is positive when the wing is dorsal, and negative when ventral. The angle of elevation θ is positive when the wing lies above the stroke plane.

2.3.4. *Wingbeat frequency*

The time interval between frames was determined from the 1 ms timing marks placed on the film by the camera. Although a significant time elapses before the camera reaches steady running speed, film acceleration is nearly constant during a sequence and the time intervals were adjusted for this. The wingbeat frequency n was measured between two successive pronations at the moments when the wing chords were perpendicular to the stroke plane. This position could be determined with good temporal accuracy because pronation is very rapid, and the moment was chosen between two frames by visual interpolation if necessary. The accuracy of the frequency measurement is about $\pm 2\%$.

Before ending this section, some general comments on the analysis procedure might be appropriate. The basic requirements for the method are (i) a long focal length lens, (ii) a single-view film sequence showing symmetrical flight and (iii) a maximum projection of the wing length, (iv) negligible bending along the longitudinal wing axis, and (v) either patience with laborious calculations or an on-line computer system. The initial investment of time in developing the film analysis system and writing programs was considerable, but the complete kinematics for one wingbeat could then be obtained in little more than an hour, including digitizing, analysis, print-out and plotting of results.

3. Results and discussion

The performance of the agitated insects inside a bare flight chamber under glaring lights was surprisingly similar to their flight behaviour in the wild. The drone-fly *Eristalis tenax* seemed least affected by the unnatural conditions, and would often hover near the centre of the chamber during the filming. The hover-fly *Episyrphus balteatus* gave a similar performance, but sometimes stopped its wingbeat and dropped to the bottom of the chamber in protest to the lights. Excellent film sequences were obtained for both of these territorial dipterans, showing the precise hovering that is characteristic of them in this field. The honey bee *Apis mellifera*, bumble bees *Bombus*, and the cuckoo bee *Psithyrus vestalis* hover with slightly less accuracy, and their manoeuvres are slower and clumsier in confined spaces. A few very good films were obtained of these insects ponderously flying around the chamber, but they often collided with the chamber walls during the films, probably because of disorientation by the lights.

The crane-flies *Tipula obsoleta* and *T. paludosa* are slow steady fliers showing little manoeuvrability, and they normally 'hover' only for brief moments when changing the direction of flight. This behaviour was also found in the flight chamber: they inspected the cage using slow flight, concentrating on its top and side boundaries. The plume moth *Emmelina monodactylus* is also a slow flier, but has a more erratic flight path and is more manoeuvrable than the crane-flies. Inside the flight chamber it quickly landed on a side wall, and no films of hovering were obtained.

I have never observed the Mediterranean flour moth *Ephestia kuehniella* in nature, but it gave a dazzling aerobatic display inside the flight chamber: loops, 180° banked turns within the course of 2 wingbeats, and Immelmann turns (a half-loop followed by a half-roll to reverse the direction of flight). I suppose that many of the pyralid moths, with their low wing loadings, can match this performance. During this entertainment there were no sequences that could be construed as hovering, even by the most flexible of definitions.

The green lacewing *Chrysopa carnea* is also very manoeuvrable in the flight chamber and can change the direction of flight in a single wingbeat, as can the other neuropteran *Pterocroce capillaris*. Even when filmed during take-off, the flight was too fast to be considered as hovering: it would accelerate to fast flight during the first wingbeat. This performance may seem somewhat surprising since *Chrysopa* is typically a slow flier, but a great manoeuvrability would certainly be advantageous in escaping from bats, their main predators.

The seven-spot ladybird *Coccinella 7-punctata* is a medium-speed steady flier that exhibits gentle manoeuvres. I have never observed it hovering in the field, but its ability to take off vertically indicates that it should be able to do so. When filmed during take off it usually entered a banked spiral, losing altitude while gaining speed, and finally levelling out if it had not collided with the chamber wall by that time. A few take-offs showed straight flight with no loss of height, however, and one of these was slow enough to be considered as hovering. During flight the elytra flapped through a small angle (about 15–20°) in phase with the hindwings. This has been found for other Coleoptera and is probably a passive movement accompanying the beating of the hindwings (Stellwaag 1914; Magnan 1934; Burton & Sandeman 1961). Because the amplitude of flapping and the size of the elytra are small compared with the hindwings, their aerodynamic effect in hovering will be neglected.

3.1. *What is hovering?*

Only a very few of the film sequences can be classified as 'hovering' according to a pedantic definition, that the mean wing force is exactly vertical and precisely balances the weight of the insect. In practice, however, flight at low velocities and low accelerations can be regarded as hovering because the kinematics and aerodynamics will not be significantly different. A less formal definition of hovering, even if an arbitrary one, is clearly needed for selection of the film sequences. This definition must accord with the aims of the investigation and hence select sequences where *the wing kinematics produce forces that are very similar to 'true' hovering*.

3.1.1. *Manoeuvres*

Animals often appear to 'hover' briefly while changing the direction of flight, but the wings are generating acceleration forces in these periods. For some of the films I doubt if steady flight was ever achieved: the insects continuously manoeuvred around the flight chamber and 'hovered' only during these fleeting moments. Do such *accelerations* represent a significant departure from hovering?

Manoeuvres were usually confined to the horizontal plane and were remarkably similar for the different insects. (The hover-fly *Episyrphus* is omitted from this discussion because films of manoeuvres are lacking.) The horizontal changes in flight direction and velocity were always *preceded* by a tilt of the stroke plane: β was increased as the insects accelerated forward, and decreased, usually becoming negative, as they decelerated or began backward flight. Similarly, accelerations in lateral directions were accompanied by a roll of the stroke plane. The obvious analogy between this type of control and that used for helicopters is quite valid. Consider a hovering insect that changes β to accelerate into forward or backward flight. The flight velocity is small during the initial stage of acceleration, and the airflow around the wings will still be governed largely by the flapping velocity. The aerodynamic forces relative to the stroke plane will be unchanged, and so the vertical hovering force will simply be rotated through the same angle as the stroke plane. This agrees with Hollick's (1940) results for tethered *Muscina stabulans*

in still air: the resultant force was nearly perpendicular to the stroke plane for any body orientation. The horizontal thrust component of the rotated force will be $mg \sin(\beta - \beta_0)$, where β_0 is the value for hovering and m is the total mass, and the vertical component will be $mg \cos(\beta - \beta_0)$. Small tilts of the stroke plane will thus produce substantial horizontal thrusts and accelerations, while the vertical force component supporting the weight is almost unaffected: a tilt of but 10° generates a thrust of 0.17 *mg*, which would accelerate the insect to a velocity of 1.7 m s^{-1} in just 1 s, but the vertical force is decreased by only 0.015 *mg*.

Most of the observed manoeuvres fit this description quite well – the vertical hovering force *mg* is simply rotated through a small angle – and we may conclude that they are not significantly different from hovering. Very brisk manoeuvres may require horizontal forces comparable with the weight of the insect, however, and cannot be considered as hovering: some sequences of *Ephestia* and *Chrysopa* even demanded thrusts of between two and five times the weight. The stroke plane was tilted through large angles for these cases, and the net force from the wings must have been much greater than *mg*.

3.1.2. *Steady flight*

Consideration of the mean forces required for steady flight leads to a similar conclusion: the mean force is hardly different from that of hovering at any flight speed. In steady flight, the horizontal thrust balances the body drag of the insect. Weis-Fogh (1956) found that a thrust equal to 0.06 *mg* was needed for locusts flying at 3.5 m s^{-1}, and Vogel (1966) measured values of 0.07 and 0.18 *mg* for *Drosophila* flying at 1 and 2 m s^{-1}, respectively. Rough calculations for my insects reveal that similar thrusts are required for fast forward flight: less than 0.1 *mg*. In all of these cases the total force demanded of the flapping wings does not exceed 1.02 *mg*. This force is largely vertical with a forward tilt of less than 10°, and usually less than 5°. For both steady and accelerated flight it is obvious that the mean force differs little from that for hovering; mean force is thus an insufficiently selective criterion for choosing film sequences to illustrate 'hovering'.

A strong correlation between flight speed and body angle χ has been demonstrated for *Drosophila* (Vogel 1966; Götz 1968; David 1978) and the honey bee (Nachtigall *et al.* 1971; Esch *et al.* 1975): the body angle is large in hovering and becomes more horizontal as flight speed increases. This behaviour is also evident on my films when steady flight at various speeds can be observed. (Unfortunately, steady flight at different speeds was not observed for the interesting case of the hover-fly *Episyrphus*, which can hover with a nearly horizontal body.) The angle between the stroke plane and the body axis is constant for *Drosophila* (Vogel 1966) and slightly variable for the honey bee (Stellwaag 1916; Neuhaus & Wohlgemuth 1960), so these results indirectly show that the stroke plane rotates with the body and becomes more vertical with increasing flight speeds. Greenewalt (1960) has found a direct correlation between β and flight velocity for hummingbirds as well. Vogel (1966) interpreted this phenomenon as an actuator disc with variable tilt; the direction of the resultant wing force, and hence its vertical and horizontal components, is controlled by the tilt of the stroke plane. For accelerations at low flight speeds, as discussed above, this is quite valid and the resultant force simply rotates with β. His interpretation is misleading for steady flight at higher speeds, however, because the resultant force rotates through a much smaller angle than the stroke plane, as Weis-Fogh (1956) had previously noted. The stroke plane rotates through about 40–60° from hovering to fast forward flight for the insects considered (excluding *Episyrphus* again), but the resultant

force tilts by less than 10°. A more direct explanation of the large changes in β lies in the asymmetry of upstroke and downstroke forces introduced by the flight velocity, and this will lead us to a definition of hovering.

3.1.3. *Advance ratio*

Figure 5*a* shows three versions of the path through the air of a wing flapping in two-dimensional motion at a stroke plane angle of 20° (the motion is sinusoidal and the effects of the induced velocity are ignored, but these details do not qualitatively affect the arguments). The paths

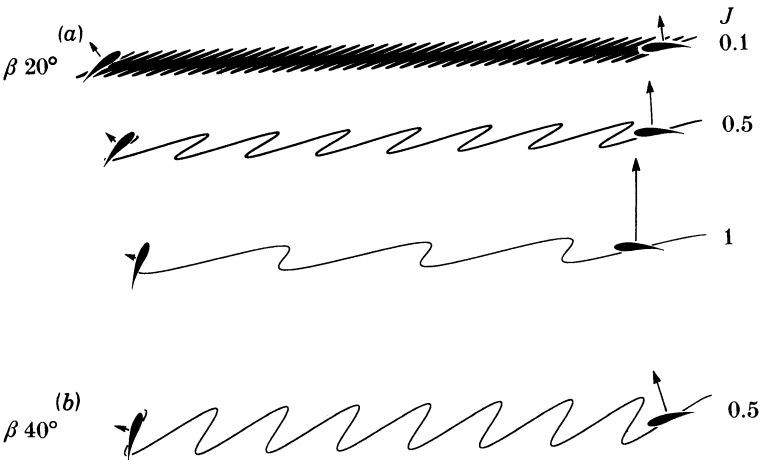

FIGURE 5. The path through the air for a wing flapping in two-dimensional motion from right to left, at different values of the stroke plane angle β and advance ratio J. Downstroke forces are shown on the right, upstroke on the left. A lift:drag ratio of 4 is arbitrarily assumed. (*a*) $\beta = 20°$. (*b*) $\beta = 40°$.

are drawn for three ratios of the flight velocity to the mean flapping velocity of the wing, and by analogy to propeller theory I shall call this ratio the *advance ratio* J. As the ratio increases through the sequence, two asymmetries develop in the wing path: (i) the relative velocity of the wing on the downstroke becomes larger than on the upstroke, which is indicated by the respective path lengths, and (ii) the downstroke path is more horizontal while the upstroke is more vertical. The downstroke force progressively dominates as the advance ratio increases, since the relative velocity is larger, but the thrust component of this force becomes smaller as the path approaches the horizontal, and even negative at high ratios. The upstroke force becomes increasingly horizontal with larger values of the advance ratio, but the relatively larger thrust component is offset by the decreased magnitude of the upstroke force; at large ratios this force will have negative vertical component if lift is still generated.

Consider a stroke plane tilted away from the hovering position; the thrust will be greater than the body drag at first and the insect will accelerate forward. The net thrust is reduced as the speed increases because of the smaller *magnitude* of the upstroke force and the more vertical *direction* of the downstroke force. Hence the acceleration will decrease until an equilibrium speed is reached where the net thrust balances the body drag. Higher values of β obviously increase the initial acceleration, and they also enhance the thrust component at larger advance ratios. This is primarily due to a more inclined downstroke path, as shown in figure 5*b*, and the insect will then accelerate to a higher equilibrium flight velocity. Figures 5*a*, *b* also indicate that β influences the type of asymmetry introduced by the flight velocity: the velocity difference

between half-strokes is greater when β is small, and the direction of the wing paths is most different for large values of β.

These deliberations have been directed towards animals that hover with a horizontal stroke plane, the hummingbirds and most insects, but the principles are more generally applicable. The stroke plane angle β must increase with the advance ratio J to produce a wing path that, when combined with the lift:drag ratio of the wings, results in the required mean force. This process necessarily entails an asymmetry between half-strokes as J increases, leading to the classic condition of fast forward flight where the downstroke force is completely dominant. For a definition of hovering we may take the other end of the spectrum and demand that the advance ratio be small enough that the flight velocity does not introduce a significant asymmetry. Judging from the wing path diagrams, I will arbitrarily define hovering as flight at values of J less than 0.1: this simply 'looks' like hovering. This value of J will alter the relative velocities on the half-strokes by less than 10% for a horizontal stroke plane, and the angles of attack by less than 6° for a vertical one. The velocity difference for small values of β may lead to a force asymmetry of $\pm 20\%$ by the quasi-steady aerodynamic assumption (paper I), but *the angles of attack will be approximately the same*: thus the force coefficients will not be affected.

The flapping velocity U varies linearly along the wing, and some representative value must be chosen to calculate the advance ratio. I suggest using the mean wing tip velocity, $\bar{U}_t = 2\Phi nR$, where the stroke angle Φ is in radians: although this is the maximum *mean* velocity, it underestimates the flapping velocities during the middle of a half-stroke, and hence gives a conservatively high estimate of J when the aerodynamic force is greatest. The advance ratio J is then

$$J = V/2\Phi nR = \hat{V}/2\Phi, \tag{23}$$

which is the inverse of Walker's (1925) parameter k. The surprising result is that for typical values of Φ, around 2 rad, non-dimensional flight velocities up to 0.4 wing lengths per wingbeat satisfy this classification of hovering. Many slow fliers, such as the crane-flies, rarely exceed this velocity range and effectively 'hover' most of the time. The power requirements for these insects must be very similar to those for 'true' hovering, which is energetically expensive because of the large induced power component. Low wing loadings and relatively large wing spans are typical of these slow fliers, and undoubtedly represent adaptations for reducing the induced power demand (see paper VI).

3.2. *The selected sequences*

Based on the considerations of the preceding section, the results from eleven film sequences are presented here as examples of hovering (figures 6–16). The top figure for each sequence contains more quantitative information than meets the eye, and will be explained with reference to the ladybird (figure 6). The stroke plane, at an angle β to the horizontal, is given by a line connecting the two opposing arrows. This line passes through the wing base axis, which is indicated by a cross on the body, and the distance from the cross to the tip of either arrowhead denotes the wing length R. The length of each arrow is the mean chord $\bar{c}$ on this scale. The side view of the body, showing the mean body angle $\bar{\chi}$, is also drawn to scale. It must be noted that the leg positions are only approximately correct, since their position had to be estimated in the sequence from a viewpoint that was rarely from the side. An arrow representing the non-dimensional flight velocity $\hat{V}$ corresponds to the wing length scale and depicts how far, and in which direction, the insect moves during a single wingbeat. The arrow is not drawn when $\hat{V}$ is less than 0.05. The magnitude of $\hat{V}$ and its direction ξ are given in the figure legend.

The roll angle η also appears in the legend, but the sign of η could not be determined for angles less than about 2°.

The wing path relative to the stroke plane is indicated by the curve, and the data points represent ϕ and θ for individual frames. Values of ϕ and θ may be read off a linear orthogonal grid, constructed with $\phi = 0$ at the wing base and $\phi = \pm 90°$ at the points of the arrowheads ($\theta = 0$ along the stroke plane). The wing path is *not* given as a simple side view, therefore. The wing attitude, drawn from visual estimation, is also presented. The angle of attack is greatest near the wing base and decreases towards the tip for all of the insects, so I have drawn the attitude around 0.7 R as representative. The chord is not properly scaled.

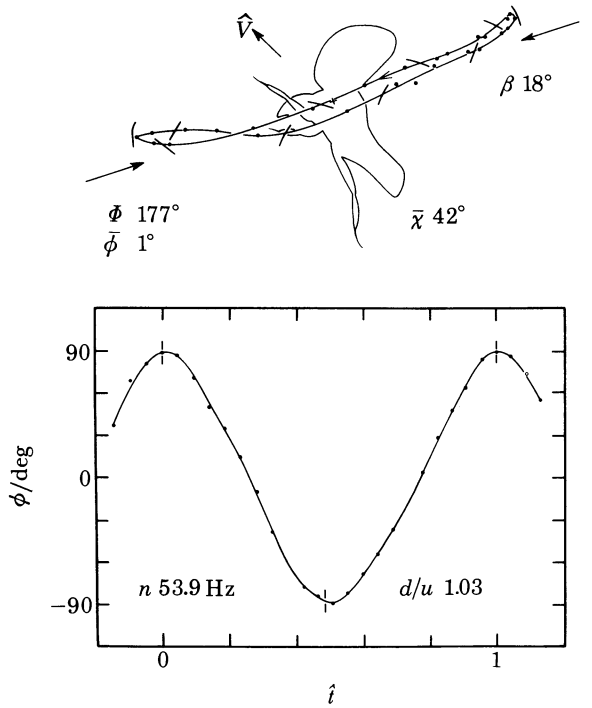

FIGURE 6. Results for the ladybird *Coccinella 7-punctata* (LB04). $\hat{V} = 0.19$, $\xi = 44°$, $\eta = 20°$. The aerodynamic role of the elytra, shown projecting above the body in this side view, should be negligible in hovering.

The lower drawing shows the positional angle ϕ plotted as a function of non-dimensional time $\hat{t}$ ($= nt$); the curve is drawn by eye. The vertical bars on the graph indicate the middle of pronation (near ϕ_{max}) and the middle of supination (near ϕ_{min}). The wingbeat frequency n and the ratio of duration of downstroke to upstroke d/u are given on this graph; the stroke angle Φ ($= \phi_{max} - \phi_{min}$) and the mean positional angle $\bar{\phi}$ appear above it. The open circle on the graph indicates the frame showing the maximum projected wing length. In the error analysis the coordinates of this point are shown to be unreliable, so it is not included in the wing path of the top figure. The results generally confirm the predictions of the error analysis. Departures from the expected errors are usually attributable to frames showing an edge-on view of the wing, where the wing tip position could not be absolutely identified: in some frames the position was so ambiguous that data were not taken.

The ladybirds (figure 6), crane-flies (figures 7, 8), honey bees (figure 14) and bumble bees (figures 15, 16) all hover with a horizontal stroke plane, but it cannot be determined from the

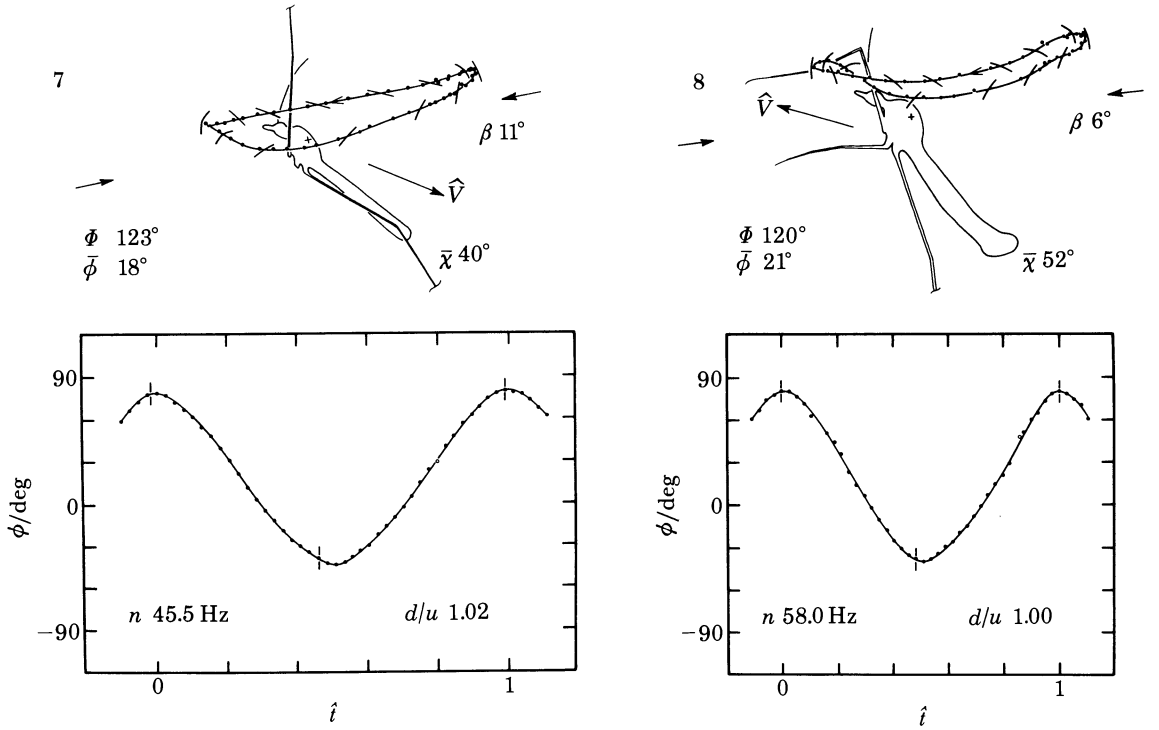

FIGURE 7. Results for the crane-fly *Tipula obsoleta* (CF02). $\hat{V} = -0.40$, $\xi = -23°$, $\eta = 2°$.

FIGURE 8. Results for the crane-fly *Tipula paludosa* (CF04). $\hat{V} = 0.39$, $\xi = 17°$, $\eta = 7°$.

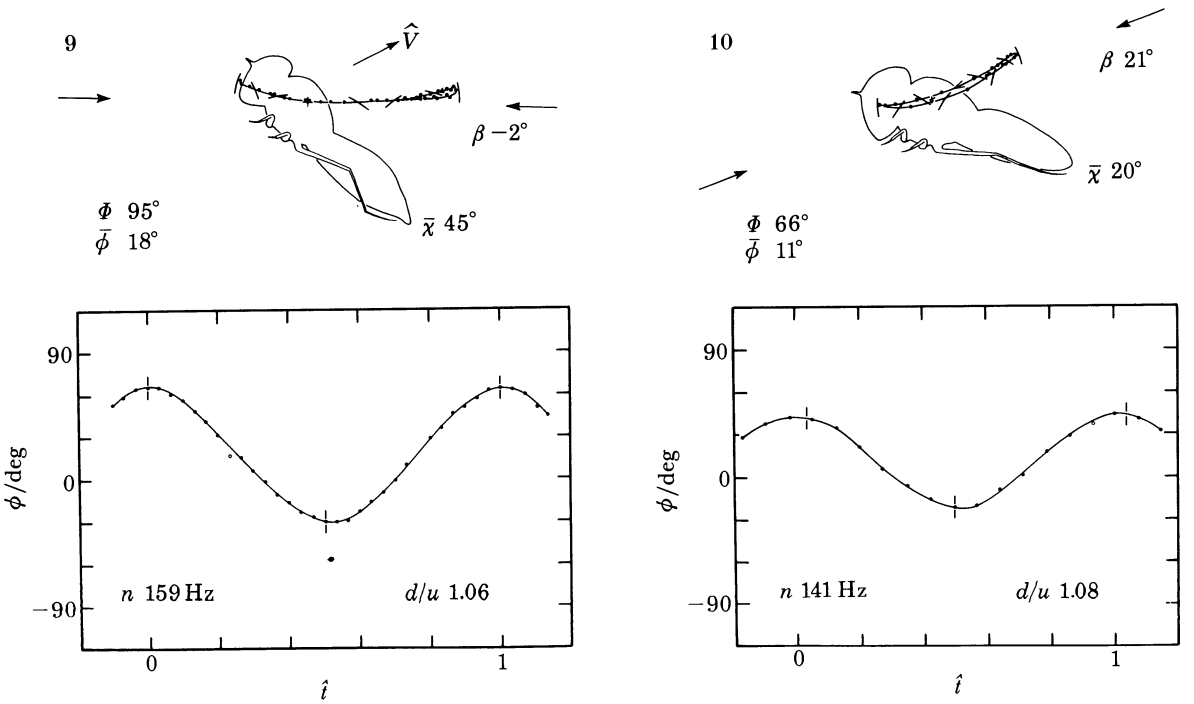

FIGURE 9. Results for the hover-fly *Episyrphus balteatus* (HF07). $\hat{V} = -0.24$, $\xi = 26°$, $\eta = 1°$.

FIGURE 10. Results for the hover-fly *Episyrphus balteatus* (HF08). $\hat{V} = 0.03$, $\xi = -1°$, $\eta = 2°$.

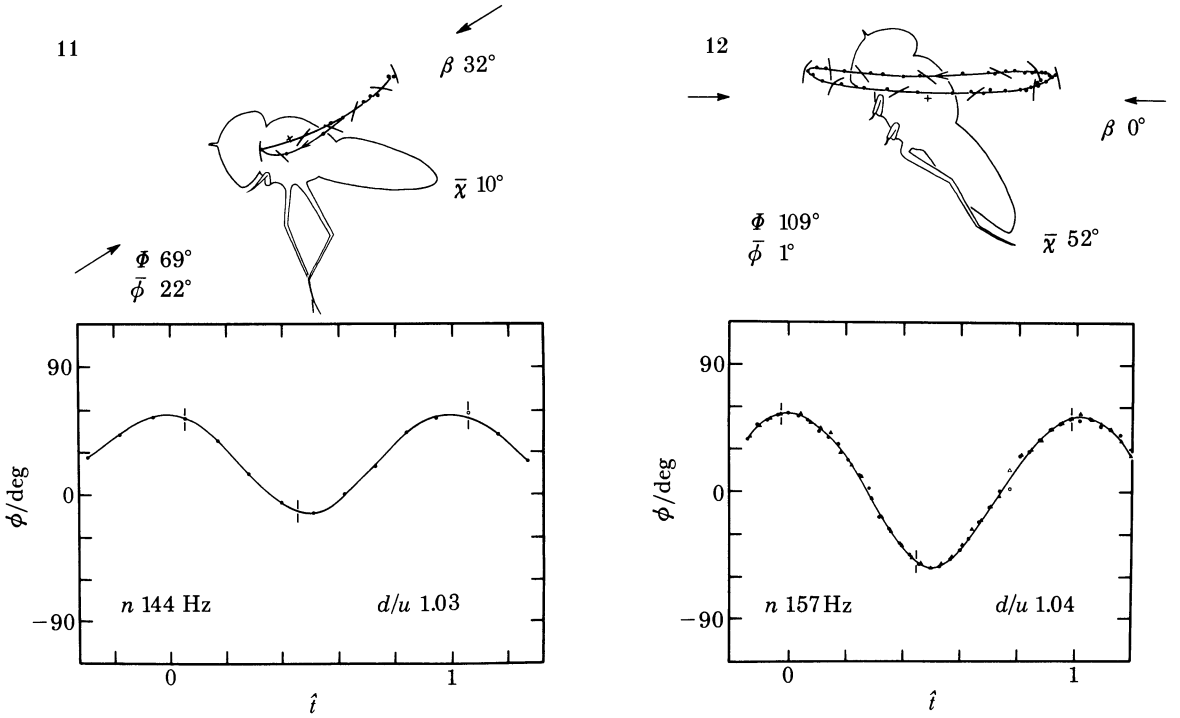

FIGURE 11. Results for the hover-fly *Episyrphus balteatus* (HF08). $\hat{V} = -0.03$, $\xi = -16°$, $\eta = 1°$.

FIGURE 12. Results for the drone-fly *Eristalis tenax* (DF01). $\hat{V} = -0.05$, $\xi = -6°$, $\eta = 3°$. Two cycles are plotted on the lower diagram because of some uncertainty in the wing tip position during film analysis.

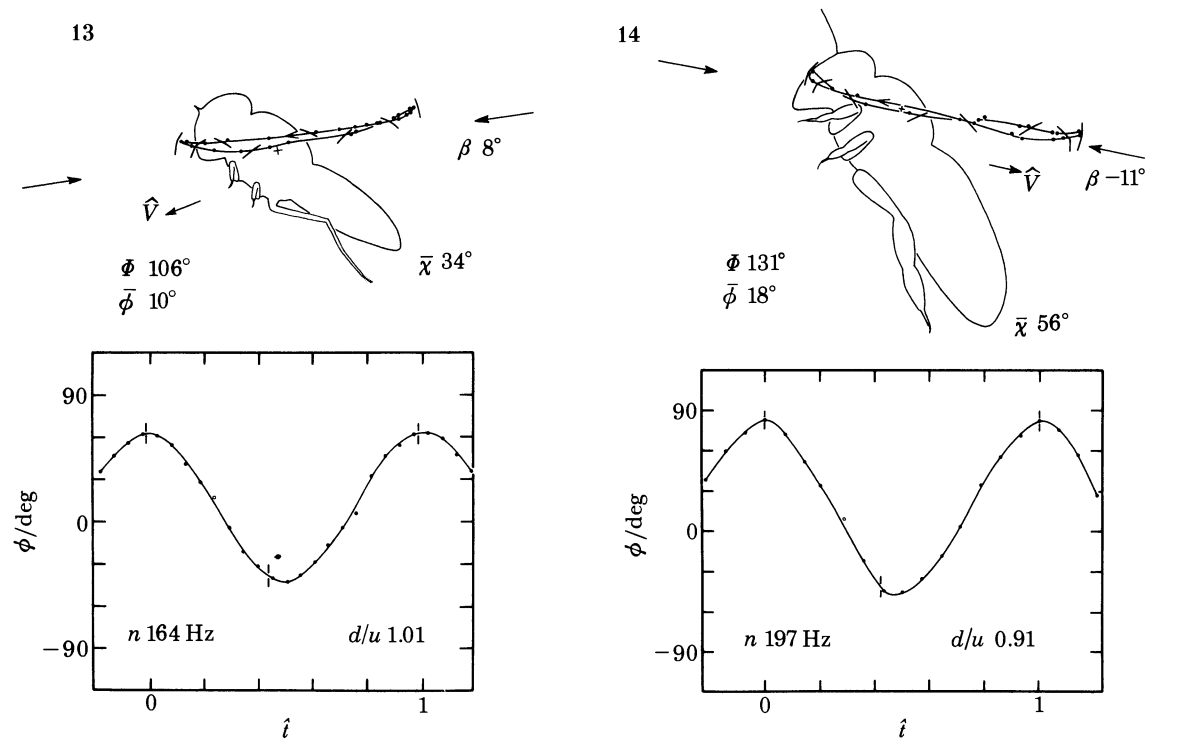

FIGURE 13. Results for the drone-fly *Eristalis tenax* (DF01). $\hat{V} = 0.18$, $\xi = -20°$, $\eta = 2°$.

FIGURE 14. Results for the honey bee *Apis mellifera* (HB01). $\hat{V} = -0.18$, $\xi = -13°$, $\eta = 6°$.

films if β is actually zero during hovering. From §3.1.1 it is obvious that β will be affected by the almost continuous manoeuvres inside the flight chamber, and we must be content to note that β is not far from zero for the selected sequences. The ladybird (figure 6) shows the greatest deviation, with $\beta = 18°$, but this sequence shows the insect steadily accelerating forwards and upwards seven wingbeats after take-off: this value of β largely accounts for the forward acceleration. Similarly, non-zero values of the roll angle η are responsible either for lateral accelerations or for properly banked turns at steady flight speeds.

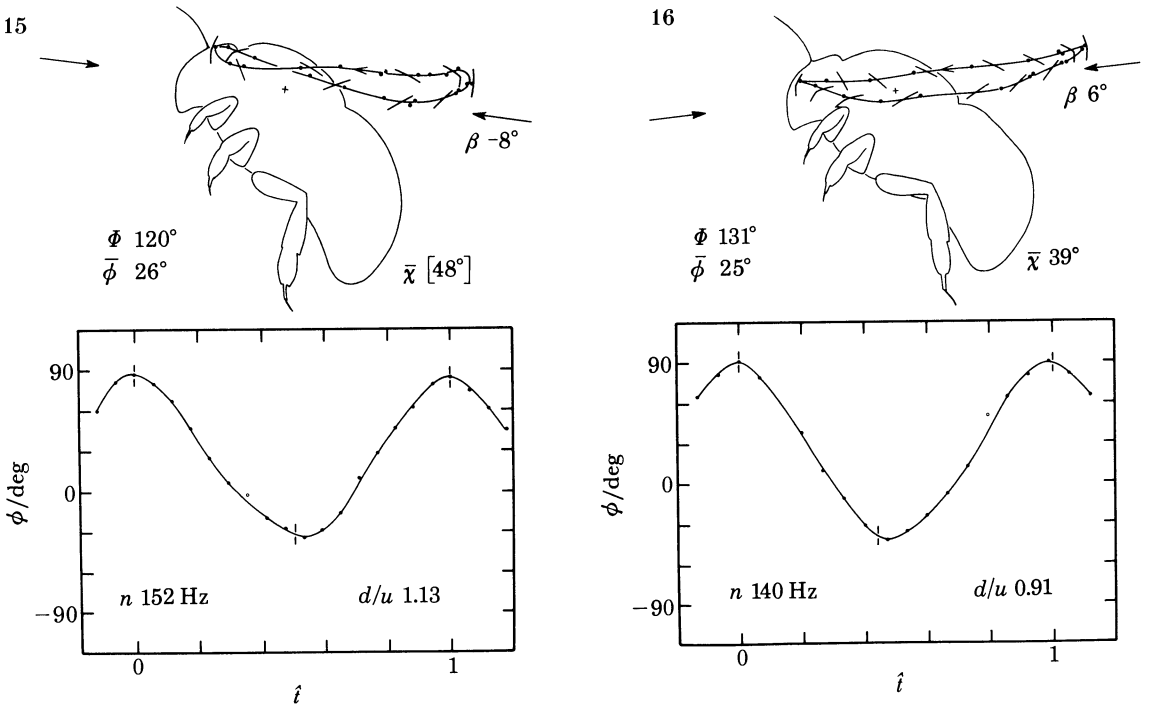

FIGURE 15. Results for the bumble bee *Bombus hortorum* (BB04). Because of a nearly front view, the flight velocity and body angle could not be determined accurately from the kinematic analysis. The insect appears to be climbing vertically, but the flight velocity $\hat{V}$ is only about 0.01. $\eta = 2°$. Mean body angle $\bar{\chi}$ is estimated from the projected body length.

FIGURE 16. Results for the bumble bee *Bombus lucorum* (BB08). $\hat{V} = -0.02$, $\xi = 21°$, $\eta = 10°$.

The drone-fly *Eristalis* habitually hovers with a horizontal stroke plane, and can vary the angle between the stroke plane and the body by up to 10° (figures 12, 13). I have also observed this dipteran occasionally hovering with an inclined stroke plane in the field, but it would not do so in the laboratory. This provides an interesting contrast to the hover-fly *Episyrphus*, which prefers to hover with an inclined stroke plane but can hover equally well with a horizontal one. The three hover-fly sequences (figures 9–11) have captured this range, showing hovering with values of β of −2°, 21° and 32°. The angle between the stroke plane and the body axis is, however, roughly constant for these examples.

The stroke angle Φ for various insects has already been discussed by Weis-Fogh (1973), and the values presented here are in close agreement. It is about 120° for most insects, but nearly 180° for *Coccinella* and other Coleoptera. Hover-flies using an inclined stroke plane are at the other end of the spectrum with very small stroke angles: 66–69°.

3.3. *Kinematics of the body*

3.3.1. *Oscillations of body position*

The phasic wing forces produce very little cyclic movement of the body on the film sequences. The position of the wing base in the plane of symmetry coordinate system (x', y', z') was calculated according to the mean flight speed $\hat{V}$ and direction ξ, and then subtracted from the observed position in each frame to give the deviations of the vertical $\Delta z'$ and horizontal $\Delta x'$ positions from the mean motion. For all of the insects except the ladybird these deviations were about ± 1–$2\,\%$ of the winglength: this is comparable with the measurement accuracy for body position, and so phasic variations in x' and z' could not be detected. In fact, a scaling argument shows that the magnitude of these deviations should remain a simple proportion of the wing length for all hovering animals, using the quasi-steady aerodynamic analysis of paper I. Based on the assumption that the aerodynamic forces are proportional to wing area and the square of the flapping velocity, the amplitude of positional *accelerations* is proportional to n^2R^4/m, where n is wingbeat frequency, R is wing length and m is total mass. Integrating this relation twice with respect to time then proves that the amplitude of oscillations in body *position* is proportional to R^4/m and, quite surprisingly, is independent of wingbeat frequency. Since wing length is generally proportional to $m^{\frac{1}{3}}$ (Greenewalt 1962, 1975), the amplitudes of $\Delta z'$ and $\Delta x'$ are therefore proportional to wing length.

Figure 17*a* presents the deviations $\Delta z'$ and $\Delta x'$ for the ladybird sequence (figure 6); they are about $\pm 3\,\%$ of the wing length and show an interesting variation over the cycle. The vertical position $\Delta z'$ tends to lag slightly behind the mean value on the downstroke and lead it on the upstroke, and the situation is reversed for the horizontal position $\Delta x'$. The cyclic wing forces must lead these changes in position by 180°, so the results indicate that the downstroke provides a greater vertical force while the upstroke generates a larger horizontal thrust. This difference between the half-stroke forces is due to the tilted stroke plane: the *net* wing force may simply rotate with the stroke plane during accelerations but, because of wing drag, the relative proportions of vertical and horizontal components will be altered for the half-stroke forces. As β increases, the partitioning of the roles of weight support and thrust becomes more pronounced, and must lead to greater oscillations in the body position. The ladybird sequence has the largest value of β for the insects that 'hover' with a horizontal stroke plane, and this may explain why phasic variations in body position were found only for that case.

3.3.2. *Oscillations of body angle*

Oscillations of the body angle χ also proved to be small in general; the amplitude is less than $\pm 1°$ for the Hymenoptera and higher Diptera, $\pm 2°$ for the tipulids, and $\pm 3°$ for the ladybird. A cyclic variation can be detected for the larger amplitudes, and this is illustrated in figure 17*b* for the crane-fly sequence (figure 7). The maximum and minimum body angles are found near the dorsal and ventral ends of the stroke, respectively, which implies that the greatest nose-down pitching moments are produced near the dorsal end while the nose-up moments occur around the ventral end. The flapping wings generate pitching moments from (i) the lift force acting on the wing length, especially when the wings are near either end of the stroke, (ii) the drag force acting on the small moment arm between the wing bases and the centre of mass, and (iii) the inertial wing forces (mass and virtual mass) acting on that same moment arm. The lift-produced moments are the only ones consistent with the phase of the

body oscillations, however: the other moments would yield extreme body angles either during the middle of half-strokes (ii) or else at the ends but reversed in direction (iii). This result may seem surprising since the lift force must fall to small values at either end of the wingbeat, but the large moment arm afforded by the wing length must more than compensate for this. When viewing Weis-Fogh's films of the tiny wasp *Encarsia*, I have noticed that the body angle oscillates much more than for most insects, and this is undoubtedly a consequence of the 'fling' mechanism (Weis-Fogh 1973): the dorsal fling particularly enhances the wing lift at that end of the cycle, and must generate large pitching moments. My films of other insects that perform a fling (*Ephestia*, *Emmelina* and the Large Cabbage White butterfly *Pieris brassicae*) suggest that this observation is more generally true.

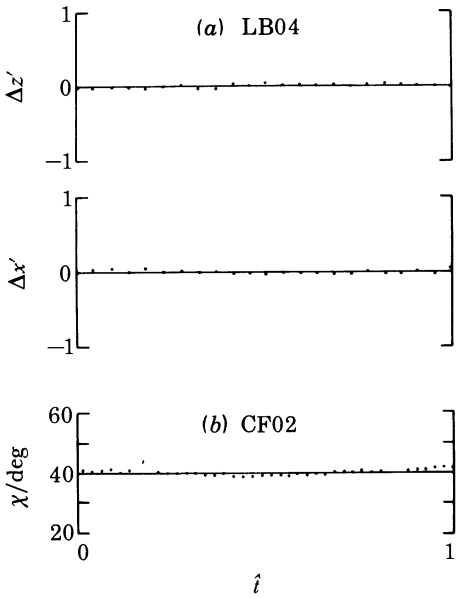

FIGURE 17. (*a*) Deviations of the vertical $\Delta z'$ and horizontal $\Delta x'$ positions of the wing base from the mean flight path for the ladybird sequence (figure 6), expressed as fractions of the wing length and plotted against cycle time. (*b*) Body angle χ for the crane-fly sequence (figure 7) during the cycle.

3.3.3. *Pitching moments, mean body angle and manoeuvres*

Since the pitching moments from wing lift appear to be the dominant ones, they should also govern the mean body angle $\overline{\chi}$. The mean moment about the wing base axis required to maintain $\overline{\chi}$ is $mgl_1 \sin(\overline{\chi}-\chi_0)$, where χ_0 is the free body angle and l_1 is the distance from the wing base axis to the centre of mass (see paper II). For nearly all of the insects $\overline{\chi}-\chi_0$ is negative, and a mean nose-down pitching moment is therefore demanded from the wing lift. This requires that the *centre of lift* over the wingbeat must be located dorsally, which accords with the positive values found for the mean positional angle $\overline{\phi}$. Thus the insects can control the mean pitching moment, and hence the mean body angle, simply by the mean angular position of the flapping wings.

The two *Eristalis* sequences offer support for this interpretation of the role of $\overline{\phi}$. In figure 12, $\overline{\phi}$ and $\overline{\chi}-\chi_0$ are only 1° and 2° respectively; neither value is significantly different from zero. The wing motion is symmetrical in the dorsoventral direction and no mean pitching

moments are required to maintain the mean body angle, which indicates that the net pitching moment is indeed zero when $\overline{\phi} = 0$. In the other *Eristalis* sequence (figure 13) the wing motion is shifted dorsally, with $\overline{\phi} = 10°$, and the mean nose-down pitching moment that this should produce agrees with a reduction in the mean body angle from 52° to 34°. A similar conclusion may be drawn from the two *Episyrphus* sequences (figures 10, 11), where a dorsal shift in $\overline{\phi}$ again corresponds to a decreased body angle. The results for the third hover-fly sequence (figure 9) cannot, however, readily be explained. Only a small nose-down pitching moment is demanded of the wings since $\overline{\chi}$ is close to χ_0, but the dorsally shifted wingbeat *should* produce a large moment. Perhaps this moment did exist and was used to rotate the body and stroke plane nose-down, halting the backward flight by the consequent forward thrust. Unfortunately I cannot tell because, like the proverbial fish that got away, the film ended at that point. These comments on *Eristalis* and *Episyrphus* provide an interesting counterpoint to Hollick's (1940) tethered studies on another dipteran *Muscina stabulans*. On interpretation of his results in light of the above discussion, he found that the centre of lift for the flapping wings also shifted with the mean positional angle $\overline{\phi}$. The pitching moments produced by this would have controlled the body angle had the insects not been tethered. *Muscina* altered $\overline{\phi}$ indirectly, however, by changing $\phi_{\min}$ while keeping $\phi_{\max}$ nearly constant; thus the mean pitching moment and the stroke angle $\boldsymbol{\Phi}$ were correlated. This contrasts with the examples above, where $\overline{\phi}$ is altered independently of $\boldsymbol{\Phi}$.

By changing the body angle, a dorsal–ventral shift in the mean positional angle will also tilt the stroke plane and hence can be used to control manoeuvres if, as discussed in §3.1.1, the angles of attack relative to the stroke plane remain unchanged. This method of control is not suitable for brisk aerobatics because the moment of inertia of the body will prevent rapid changes in attitude, but it is adequate for most manoeuvres. These comments also apply to any mechanism for altering β via $\overline{\chi}$: for the *same* longitudinal wing axis kinematics, the mean pitching moment can be changed by increasing or decreasing the lift during parts of the wingbeat cycle via the angle of attack or the robustness of a fling. The sluggishness of the body response may be circumvented to some degree by the honey bee and the drone-fly *Eristalis*, which can alter β independently of $\overline{\chi}$ to some extent. The hover-flies and other animals that hover with an inclined stroke plane may have the best solution, however: the body is already close to horizontal, and by changing the angle of attack on either half-stroke they can produce a large horizontal force for immediate acceleration. A somewhat similar mechanism seemed widely used by the filmed insects that hover with a horizontal stroke plane. To accelerate into forward or backward flight they increased the angle of attack to large values on the upstroke or downstroke, respectively, and used the increased drag to *initiate* acceleration. This 'paddling' or 'rowing' motion also rotated the body (and the stroke plane) in the correct direction because the enhanced horizontal drag force was applied above the centre of mass. As the stroke plane tilted, the increased drag would produce an undesirable negative vertical force component, and the insects reverted to more normal angles of attack after only one or two wingbeats. This mechanism for initiating accelerations was clearly evident on some films of *Tipula*, *Bombus*, *Chrysopa*, *Pterocroce*, *Manduca*, *Emmelina*, and *Ephestia*; the angle of attack on the drag-producing half-stroke often approached 90° and provided large horizontal accelerations.

3.4. *Wing tip path*

Many previous investigators have devoted attention to the path of the wing tip relative to the body: the *wing tip path*. Early work demonstrated that this path is a figure-of-eight for insects

(Marey 1873; Magnan 1934) and hummingbirds (Stolpe & Zimmer 1939). Then the era of wind tunnel studies on tethered insects began, and the situation became more confused. In still air the flies *Muscina stabulans* and *Musca domestica* move their wings along simple paths (distorted ellipses with no crossings) with the upstroke anterior to the downstroke (Hollick 1940). The downstroke shifts anteriorly at flight speeds of 1.4 m s^{-1}, however, resulting in a figure-of-eight path. This is not a passive aerodynamic effect: Hollick elegantly showed that it is controlled by the airstream over the antennae, and that the extent of the figure-of-eight depends on the wind speed. Jensen (1956) found a simple path for the forewings and hindwings of the desert locust *Schistocerca gregaria* in fast forward flight, but the upstroke was posterior to the downstroke. Nachtigall (1966) described a simple path for the calliphorid fly *Phormia regina* in forward flight, and the upstroke was also posterior to the downstroke. The path flattened and crossed over near the bottom of the stroke when the wind tunnel was switched off, however, giving a slight figure-of-eight. Wood (1970) discovered a simple path for the fly *Calliphora erythrocephala* in forward flight, but the upstroke was anterior to the downstroke as in Hollick's result for still air. It is fair to say that nearly all possible combinations of figures-of-eight, simple paths, reversed directions, moving and still air have been reported.

Nachtigall (1973) also found a simple path for *Calliphora* in *free* forward flight, but the upstroke was posterior to the downstroke: the direction of this path is contrary to that reported by Wood. Nachtigall suggested that the differences in the wing tip paths may be due to method of mounting. Wood (1970) mounted the insect by the mesonotum, as had Hollick (1940). In his earlier study Nachtigall (1966) mounted *Phormia* by the tip of the abdomen, reasoning that this would least affect the thoracic mechanics. Free flight studies on *Locusta migratoria* (Baker & Cooter 1979) reveal wing tip paths similar to Jensen's (1956) locusts, which were mounted safely either by the first abdominal tergite or by the plastron. Baker & Cooter noted some variability in the wing path between and within individuals, but the path never crossed over and formed a figure-of-eight.

Because of doubts concerning the method of mounting, the wing tip paths presented here for free hovering flight should be illuminating. A figure-of-eight with the cross-over near the bottom end of the stroke is seen for the ladybird *Coccinella* (figure 6), the crane-fly *Tipula paludosa* (figure 8), and the bumble bee *Bombus hortorum* (figure 15). The other crane-fly *T. obsoleta* (figure 7) and the bumble bee *B. lucorum* (figure 16) show simple paths instead. The wing path for the honey bee *Apis* (figure 14) crosses over twice, but Neuhaus & Wohlgemuth (1960) have also reported a path with three crossings.

A smooth simple path is found for the drone-fly *Eristalis* in one sequence (figure 12), but this is flattened with a slight dorsal cross-over in the other (figure 13). A similar dorsal loop is seen for the hover-fly *Episyrphus* in figure 9, but the remaining path has collapsed into a single curve. This situation is reversed in figure 11, where the loop is ventral and the dorsal paths are coincident. Finally, a slightly open simple path is shown in figure 10 for the hover-fly.

Rather than help clarify the confusion over wing tip paths, these results from free flight only add to the problem. All of the patterns previously described are found here, except for a simple path with the upstroke anterior to the downstroke. In some cases a general wing path may exist and even be species specific: the differences between the two crane-fly species are consistent in six other films that I have analysed. Other insects, such as the hover-flies, show such a large individual variation that no general path can be detected. Previous investigators have also found variability in the wing tip paths, to greater or lesser degrees (Hollick 1940; Wood 1970; Nachtigall 1973; Baker & Cooter 1979). The exact form of the wing path is probably not very

important in flight, and we could be attaching undue significance to it simply because it is a characteristic of the complicated flight system that can be measured with relative ease. The variability is largely confined to the ends of the wingbeat cycle, where aerodynamic forces are small, and these slight changes in the direction of the wing path should not alter the net wing force significantly. Instead, the path may *indirectly* reflect control mechanisms initiated at the wing base: changes in articulation to control $\bar{\phi}, \Phi$ or the angle of attack may alter the wing tip path slightly, but more work like that of Pfau (1977) and Pfau & Nachtigall (1981) on wing base mechanics is required to test this suggestion.

3.5. *Wing motion as a function of time*

Because of the scarcity of complete kinematic data, theoretical analyses of flight usually assume that the wing position $\phi(t)$ follows simple harmonic motion. This approximation is quite accurate for the hummingbird *Melanotrochilus fuscus* (data from Stolpe & Zimmer (1939) as analysed by Weis-Fogh (1972)), but not so valid for the desert locust (Weis-Fogh 1956) and the fly *Phormia* (Nachtigall 1966). I have compared the results from this study with simple harmonic motion and found that $\dot{\phi}(t)$ is only slightly different in general: for *Episyrphus* and *Eristalis* the motion is very similar, for *Coccinella* and the tipulids it deviates but little, and the Hymenoptera differ the most. In all cases the angular velocity during the middle portion of half-strokes is reduced somewhat from the simple harmonic motion value. The accelerations and decelerations at the ends of the cycle are consequently greater, and the inertial torques must therefore be larger than the values given by the simple harmonic motion assumption.

In the quasi-steady assumption (paper I) the aerodynamic forces are proportional to the square of velocity, and so the *mean force* will be given by the mean square of the angular velocity. Furthermore, the *mean profile power* is then proportional to the mean cube of the angular velocity: it is more properly the mean cube of the absolute value of the angular velocity, since the profile power is defined as positive over the entire wingbeat. These two parameters thus offer a quantitative evaluation, with aerodynamic significance, of the departure of $\dot{\phi}(t)$ from simple harmonic motion.

It is useful to introduce a non-dimensional form of ϕ at this time,

$$\hat{\phi} = 2(\phi - \bar{\phi})/\Phi, \tag{24}$$

which ranges between $+1$ and -1 for the cycle. The angular velocity is then given by

$$\mathrm{d}\phi/\mathrm{d}t = \tfrac{1}{2}n\Phi\,\mathrm{d}\hat{\phi}/\mathrm{d}\hat{t}, \tag{25}$$

and $\mathrm{d}\hat{\phi}/\mathrm{d}\hat{t}$ is a non-dimensional angular velocity that can be used to compare different animals. I have calculated the mean square and mean cube values for $\mathrm{d}\hat{\phi}/\mathrm{d}\hat{t}$ based on the curves of figures 6–16. Such values are usually expressed as the root mean square and cube root mean cube: table 1 gives the root mean square and cube root mean cube values as well as the ratio of the mean square to that for simple harmonic motion, and the ratio of the mean cube to that for simple harmonic motion. For all insects the root mean square value is slightly less than that for simple harmonic motion, and the quasi-steady aerodynamic force estimate is only some 4% less according to the ratio of the mean square to that for simple harmonic motion. Similarly, the cube root mean cube value is smaller, and the mean profile power is generally some 9% less.

Since both the mean force and profile power are affected by the form of $\phi(t)$, we must consider

them together to gauge the net consequences of the observed wing motion. The ratio of mean lift to mean profile power can be used as one measure of the effectiveness of the wingbeat. This ratio will be determined by the function $\hat{\phi}(\hat{t})$ for given wing dimensions and flapping frequency, and it is proportional to the ratio of the mean square to the mean cube for the quasi-steady assumption. The ratio of the mean square to the mean cube of a quantity is maximum when that quantity is constant, so a given lift can be produced for minimum profile power when the angular velocity $\mathrm{d}\hat{\phi}/\mathrm{d}\hat{t}$ is uniform during each half-stroke. The form of $\hat{\phi}(t)$ observed for the insects is clearly of this tendency when compared with simple harmonic motion, and this

TABLE 1. ROOT MEAN SQUARE (r.m.s.) AND CUBE ROOT MEAN CUBE (c.r.m.c.) FOR THE NON-DIMENSIONAL ANGULAR VELOCITY $\mathrm{d}\hat{\phi}/\mathrm{d}\hat{t}$

(Insects from the selected film sequences are identified by their ID code from paper II. Values for simple harmonic motion (s.h.m.) are given for comparison. The ratios of the mean square (m.s.) and mean cube (m.c.) to the values for simple harmonic motion are also presented. Values for $|\mathrm{d}\hat{\phi}/\mathrm{d}\hat{t}|_{\max}$ and the mean of $|\mathrm{d}\hat{\phi}/\mathrm{d}\hat{t}|^{\frac{3}{2}}$ are given for use in paper VI.)

species	ID	r.m.s.	$\frac{\text{m.s.}}{\text{m.s.(s.h.m.)}}$	c.r.m.c.	$\frac{\text{m.c.}}{\text{m.c.(s.h.m.)}}$	$\left\|\frac{\mathrm{d}\hat{\phi}}{\mathrm{d}\hat{t}}\right\|_{\max}$	$\overline{\left\|\frac{\mathrm{d}\hat{\phi}}{\mathrm{d}\hat{t}}\right\|^{\frac{3}{2}}}$
simple harmonic motion	shm	4.44	1	4.72	1	6.28	45.3
Coccinella 7-punctata	LB04	4.32	0.94	4.52	0.87	5.88	41.0
Tipula obsoleta	CF02	4.26	0.92	4.46	0.84	5.90	40.1
T. paludosa	CF04	4.31	0.94	4.52	0.88	5.84	40.9
Episyrphus balteatus	HF07	4.37	0.97	4.59	0.92	6.11	42.1
	HF08 (figure 10)	4.38	0.97	4.63	0.94	6.37	43.2
	HF08 (figure 11)	4.40	0.98	4.68	0.97	6.38	45.4
Eristalis tenax	DF01 (figure 12)	4.38	0.97	4.65	0.95	6.45	43.5
	DF01 (figure 13)	4.37	0.97	4.63	0.94	6.43	43.0
Apis mellifera	HB01	4.30	0.94	4.51	0.87	6.00	41.2
Bombus hortorum	BB04	4.36	0.96	4.61	0.93	6.33	42.5
B. lucorum	BB08	4.35	0.96	4.58	0.91	6.46	43.2

is also true for many birds (Oehme & Kitzler 1974). The best case in the tipulid CF02, which shows a 10% decrease in mean profile power for a given lift force, quite a substantial saving. Conversely, the hover-flies and drone-flies benefit the least and save but 3%.

Finally, results should be noted for the ratio of the duration of the downstroke to that of the upstroke, d/u. This ratio is somewhat variable for insects but is generally greater than unity (Magnan 1934; Weis-Fogh 1956; Nachtigall 1966; Wood 1970; Baker & Cooter 1979). The values for my insects are included on the figures, and were determined from times at the ends of the half-strokes such that the $\dot{\phi}(\hat{t})$ curve was symmetrical about those times. The downstroke is slightly longer than the upstroke, which agrees with the other authors, but there are two notable exceptions: d/u equals 0.91 for the honey bee (figure 14) and a bumble bee (figure 16).

3.6 *Wing attitude*

It must be emphasized that wing attitudes were determined by *visual estimation* and cannot be regarded as very accurate. The changes in wing attitude during the course of a wingbeat are similar for *all* of the insects investigated and will be discussed in general terms. Plates

showing the film sequences for four insects will be used to illustrate the main points of this section: figure 18, plate 1, is the crane-fly sequence of figure 7; figure 19, plate 2, is the hover-fly figure 9; figure 20, plate 3, is the drone-fly figure 12; and figure 21, plate 4, is the bumble bee figure 16. Although hovering sequences were not obtained for the plume moth *Emmelina* and the lacewing *Chrysopa*, their wingbeats were similar to the other insects and are illustrated in figures 22, plate 5, and 23, plate 6, respectively.

3.6.1. *Angle of attack*

During the middle portion of each half-stroke, the angle of attack α is greatest at the wing base and decreases towards the tip: the wing is *twisted*. (The term 'angle of attack' will refer to the geometric angle of attack relative to the wing path.) This twisting may be seen in figures 18*h*, *q*, 19*f*, *o*, 20*f*, *m*, 21*g*, 22*f*, *l*, and 23 *h*. The amount of twist is very difficult to judge, because it is small, but may be around 10–20°. A similar wing twist has been found by other investigators for insects (Jensen 1956; Nachtigall 1966, 1979, 1980; R. Å. Norberg 1972*a*; Weis-Fogh 1973; Wootton 1981) and hummingbirds (Greenewalt 1960; Hertel 1966). The classical interpretation of wing twist is that it enables the wing to operate at the same angle of attack to the relative airflow along its length, like a propeller: the direction of the relative wind, composed of the flapping and induced velocities, becomes more horizontal as the flapping velocity increases towards the wing tip. Thus the twist can allow each wing section to perform at its best angle of attack. Vogel (1967*a*) found, however, that the wing is not twisted appreciably along its length for *Drosophila*. Since the lift of detached *Drosophila* wings hardly varies over the range of incidences normally encountered in flight (Vogel 1967*b*), the absence of a twist presumably is not deleterious (Weis-Fogh 1972). R. Å. Norberg (1972*b*) has suggested that wing twisting in insects may be passively produced, because the chordwise centre of lift lies posterior to the torsion axis of the wing. This seems quite likely, and it may also explain the lack of twisting in tiny insects like *Drosophila*: to judge from the small elastic deformations seen on my films of *Drosophila melanogaster*, the wings are relatively stiffer than those of larger insects and hence more resistant to torsional twisting.

It has generally been reported that the angle of attack α is set soon after the end of pronation and supination, and remains nearly constant during most of the following half-stroke. This is true for the hummingbirds (Stolpe & Zimmer 1939; Greenewalt 1960; Hertel 1966) and *Drosophila* (Vogel 1967*a*), for the downstroke of the locust *Schistocerca* (Jensen 1956), *Phormia* and a tipulid (Nachtigall 1966, 1981), and for the upstroke of the chalcid wasp *Encarsia* (Weis-Fogh 1973; Ellington 1975); α tends to increase steadily during the latter half of the downstroke for *Encarsia*, however, and it varies considerably on the upstroke of the locust, *Phormia* and the tipulid. For the insects considered here, α is nearly constant during the middle portion of each half-stroke, as can be seen on the plates. The angle of attack is normally the same on each half-stroke, and is typically about 35° at 0.7 R: it is slightly smaller for the hover-fly in figure 9, a few degrees larger for the one in figure 10, and about 30° for the drone-fly in figure 12. The angle of attack on the downstroke is less than that on the upstroke for the two crane-flies, however: α is 25° and 35° respectively for figure 7, and 35° and 45° for figure 8. For a tipulid in ascending flight, though, Nachtigall (1981) found that α is greater on the downstroke instead of the upstroke. This is also true for the hoverfly in figure 11: α is 40–45° on the downstroke and 35–40° on the upstroke.

These angles of attack are excessive when compared with the locust in fast forward flight

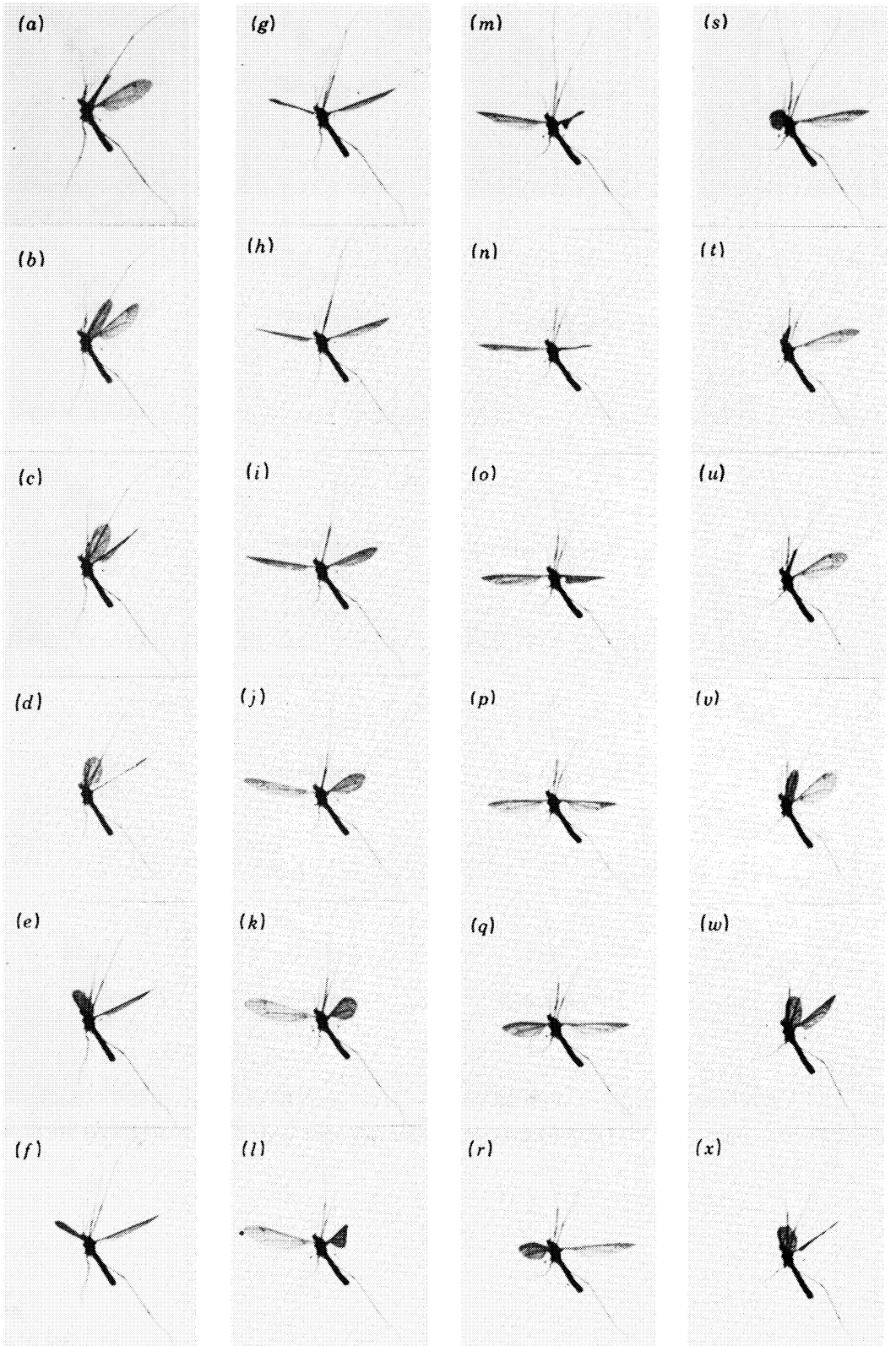

FIGURE 18. The sequence for the crane-fly *Tipula obsoleta*, used in figure 7. Alternate frames are shown.

(*Facing p.* 66)

PHILOSOPHICAL TRANSACTIONS OF THE ROYAL SOCIETY B BIOLOGICAL SCIENCES

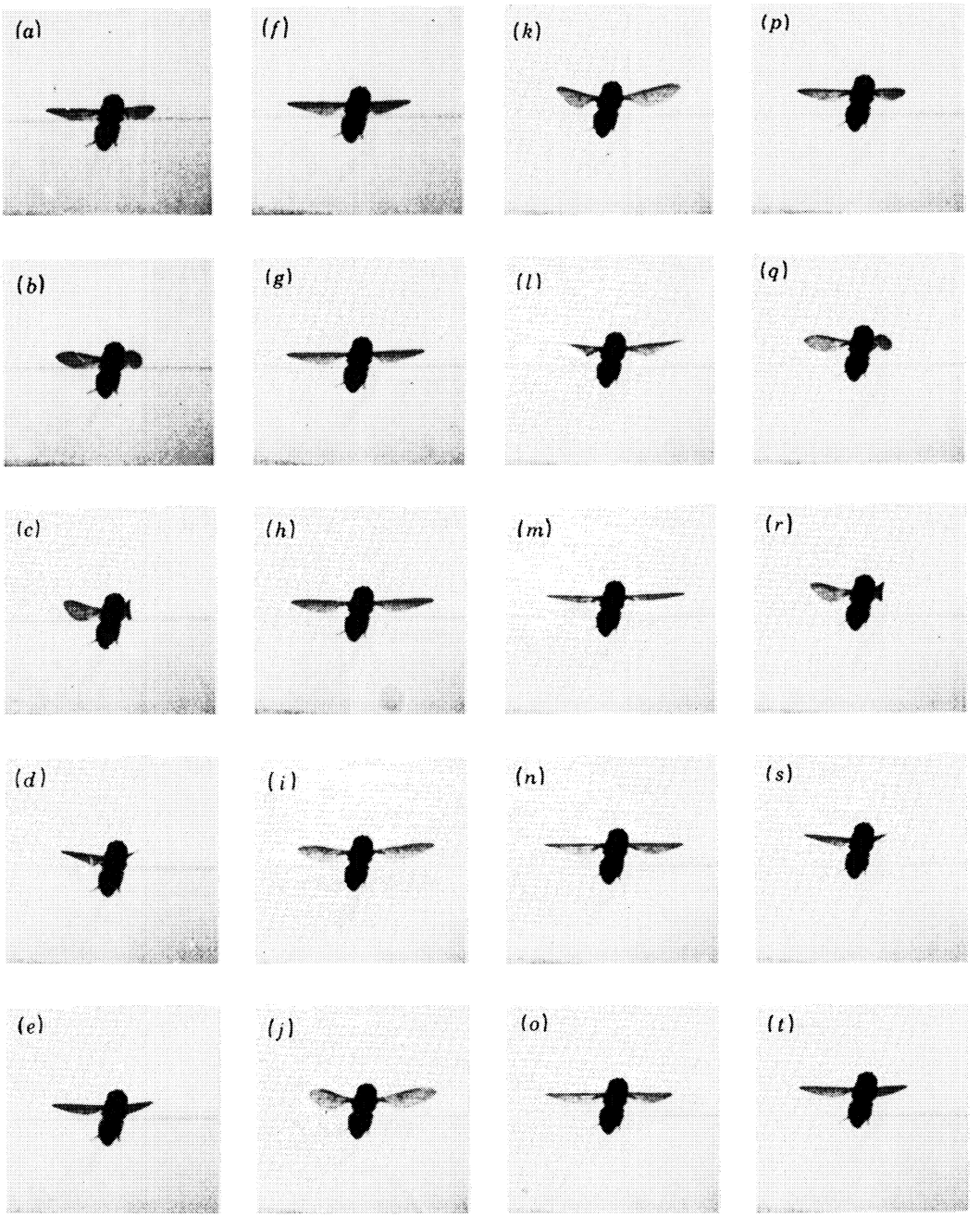

FIGURE 19. The sequence for the hover-fly *Episyrphus balteatus*, used in figure 9. Alternate frames are shown.

PHILOSOPHICAL TRANSACTIONS OF THE ROYAL SOCIETY B BIOLOGICAL SCIENCES

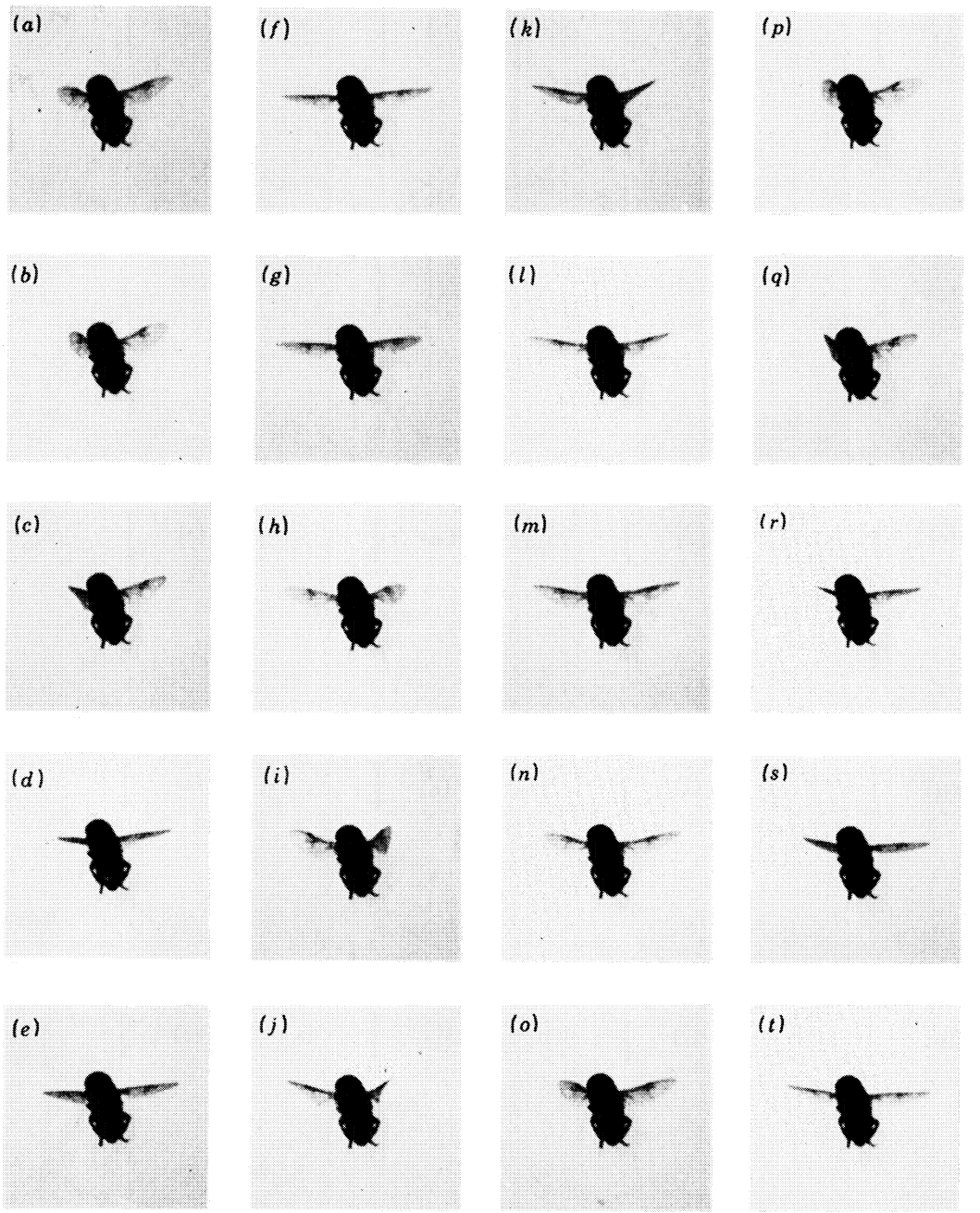

FIGURE 20. The sequence for the drone-fly *Eristalis tenax*, used in figure 12. Alternative frames are shown.

PHILOSOPHICAL TRANSACTIONS OF THE ROYAL SOCIETY B BIOLOGICAL SCIENCES

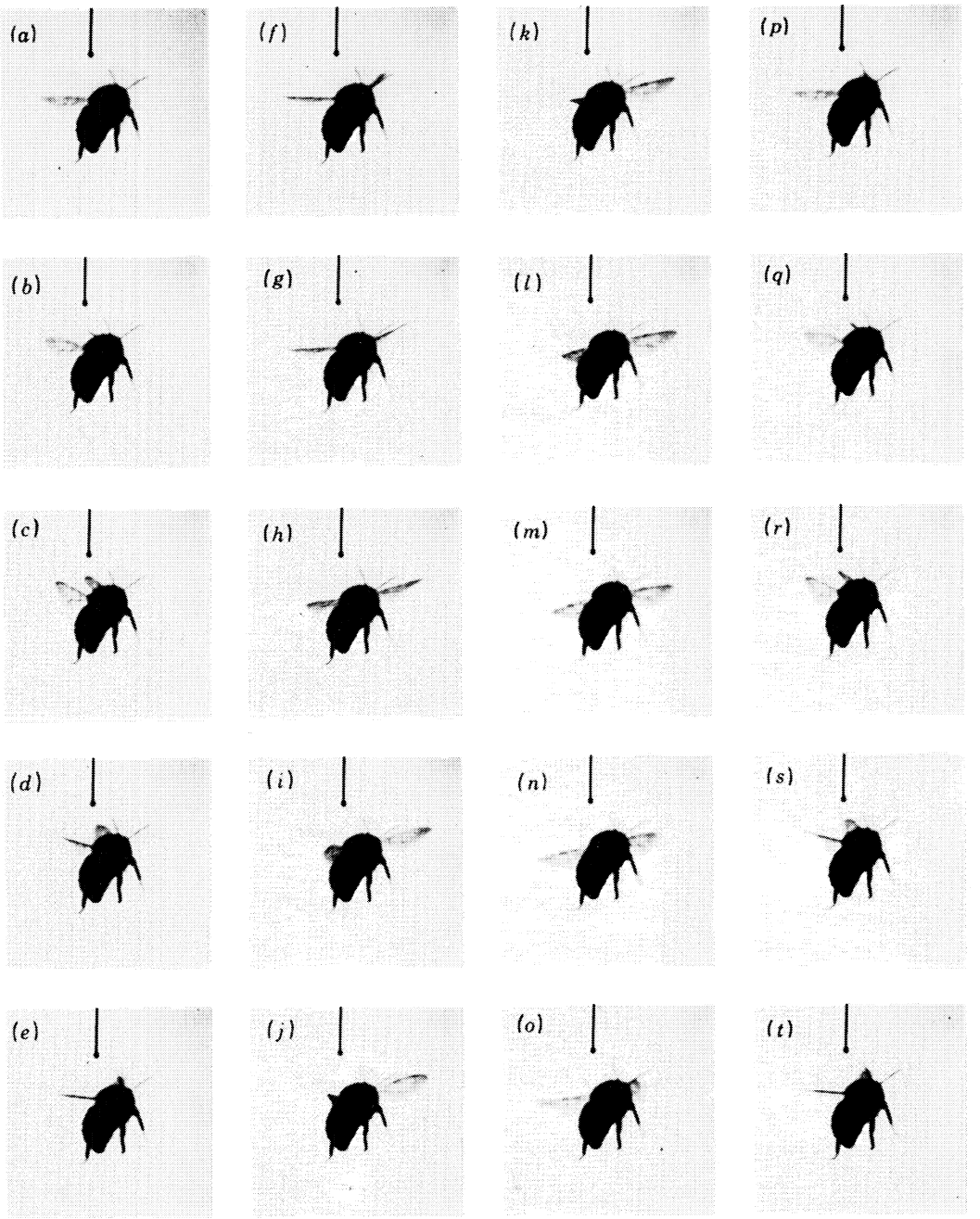

FIGURE 21. The sequence for the bumble bee *Bombus lucorum*, used in figure 16.

PHILOSOPHICAL TRANSACTIONS OF THE ROYAL SOCIETY B BIOLOGICAL SCIENCES

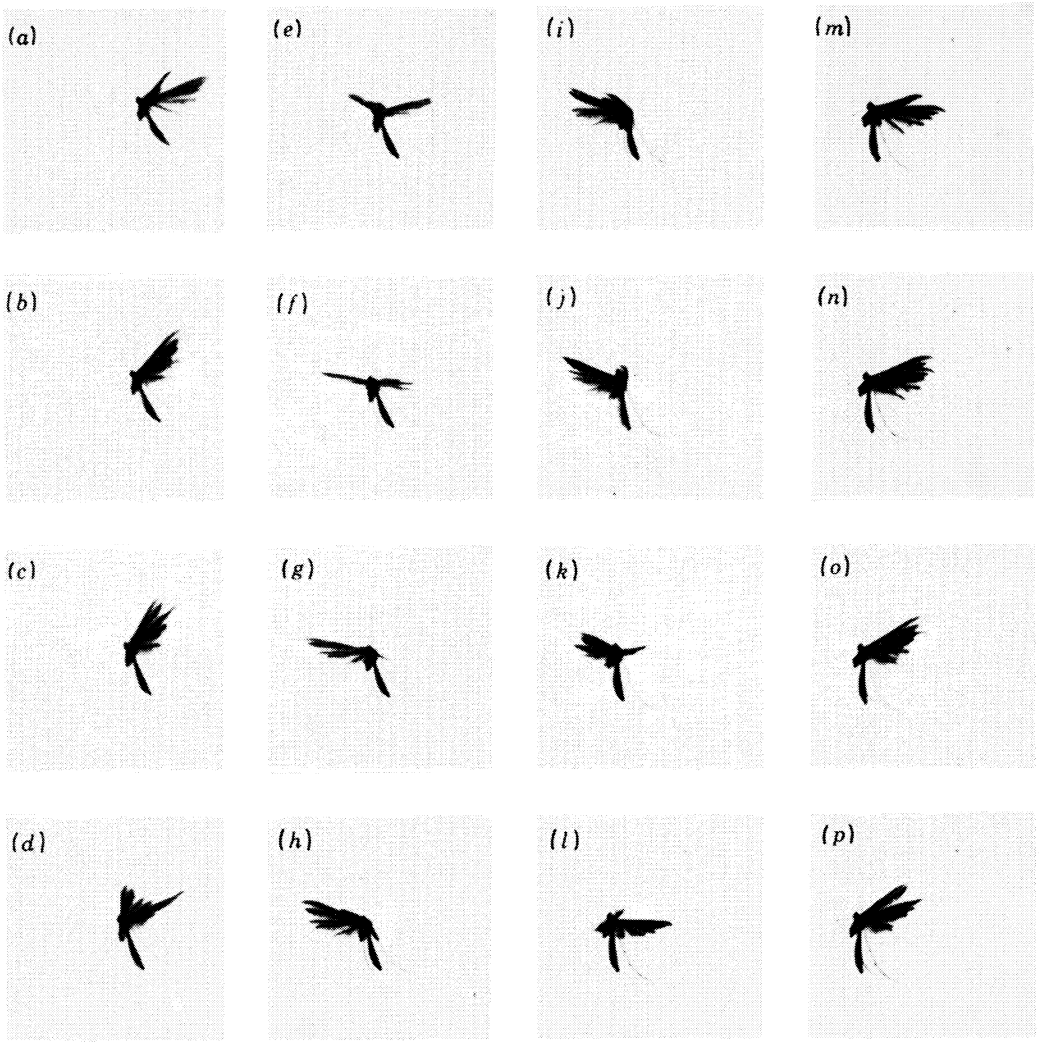

FIGURE 22. The wingbeat of the plume moth (PM01) *Emmelina monodactylus* in decelerating forward flight. Kinematic parameters: $\hat{V} = 1.42$, $\xi = -3°$, $\eta = 12°$, $\beta = 9°$, $\overline{\chi} = 59°$, $\Phi = 168°$, $\overline{\phi} = 13°$, $n = 32.9$ Hz, $d/u = 1.42$. Alternate frames are shown.

PHILOSOPHICAL TRANSACTIONS OF THE ROYAL SOCIETY B BIOLOGICAL SCIENCES

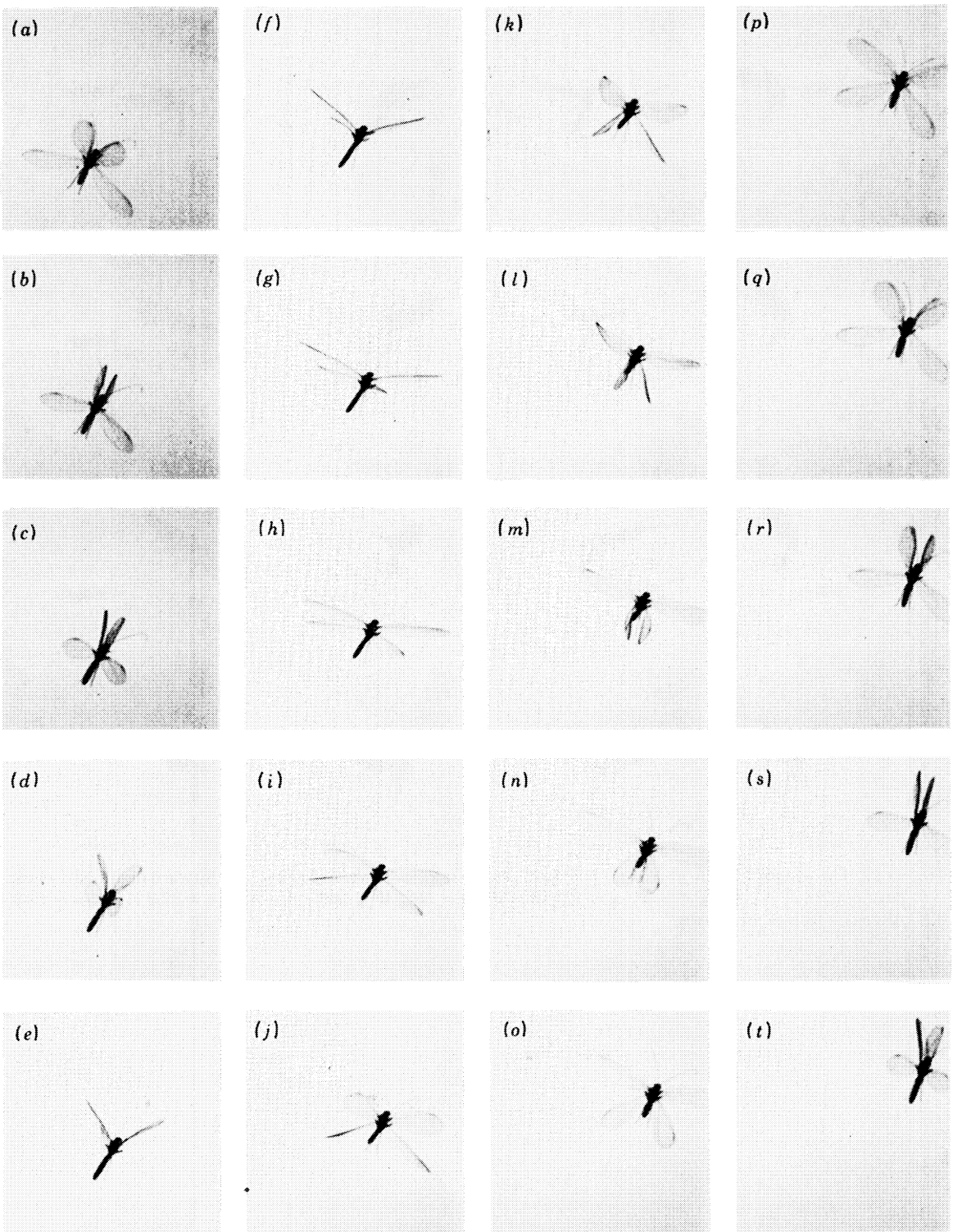

FIGURE 23. The wingbeat of the lacewing (LW02) *Chrysopa carnea* in a nearly vertical climb. Kinematic parameters: $\hat{V} = 1.2$, ξ nearly vertical, $\eta = -15°$, $\overline{\chi}$ estimated to be 60°, $n = 28.2$ Hz. Forewings: $\beta = 14°$, $\Phi = 149°$, $\overline{\phi} = 18°$, $d/u = 1.17$. Hindwings: $\beta = 2°$, $\Phi = 165°$, $\overline{\phi} = 4°$, $d/u = 0.91$. The phase relation between forewings and hindwings changes during the cycle, with the forewings leading by 0.18 of the period at pronation but 0.12 at supination. Every fourth frame is shown.

PHILOSOPHICAL TRANSACTIONS OF THE ROYAL SOCIETY B BIOLOGICAL SCIENCES

and with hovering hummingbirds, where α is less than 15° (Jensen 1956) and 25° (Hertel 1966). Although my values are visually estimated, I do not think the errors are large enough to account for the discrepancy: values similar to mine have been found for *Phormia* (Nachtigall 1966, 1979), *Drosophila* (Vogel 1967*a*), two plume moths (R. Å. Norberg 1972*a*), *Encarsia* (Ellington 1975) and a tipulid (Nachtigall 1981).

3.6.2. *Camber*

As well as the angle of attack, the wing *profile* is nearly constant during the middle portion of each half-stroke. After viewing many films, showing the wingbeat from various directions, I have formed the impression that the wings are gently cambered on both the downstroke and the upstroke, which would certainly be advantageous for animals hovering with a horizontal stroke plane. The hymenopteran wings are definitely cambered at rest, and on the downstroke of some film sequences as well. This curvature disappears on the upstroke and the wing becomes flat, if not curved slightly in the opposite direction – a feature that is more evident in plate 15 of Dalton (1977). Proximal regions of broad-based wings like *Emmelina*'s and *Ephestia*'s clearly show a reversal of curvature each half-stroke: thus the wing is always properly cambered. The photographs of two plume moths by R. Å. Norberg (1972*a*), drawings of *Manduca* (Weis-Fogh 1973), and Greenewalt's (1960) figures for hovering hummingbirds also demonstrate this reversal of curvature. For the other filmed insects, cambering in the middle of half-strokes is small and difficult to judge, bordering on the resolution of the cine films.

The wing profile has been studied for insects tethered in wind tunnels, but such results apply to fast forward flight. During the middle of each half-stroke the wings are nearly flat in general, although the forewing of the locust is bent into a **Z** profile on the upstroke (Jensen 1956). In addition, the locust deflects the posterior area of the forewing as a flap towards the end of the downstroke, and *Drosophila* similarly increases the wing camber at this stage (Vogel 1967*a*). The wing of *Phormia* is nearly flat during most of the cycle, but some camber can be seen at the initiation of the upstroke (Nachtigall 1966, 1980). The high-resolution flash photographs of Dalton (1975, 1977) provide excellent views of the wing profile, but the flight path and velocity for the insects are unknown. Cambering during the middle of half-strokes is evident to some degree on many of his photographs, as is the wing twist.

3.6.3. *Wing rotation*

As the wings begin to decelerate at the end of a half-stroke, they rotate about a longitudinal axis and increase the angle of attack. The wing tends to rotate as a flat plate – little flexing is evident – until it is perpendicular to the stroke plane. This point has been defined as the middle of pronation and supination: pronation refers to the wing rotation at the dorsal end of the cycle, and supination is at the ventral end. The bottom halves of figures 6–16 indicate the middle of pronation and supination, which generally occurs just before, or at, the end of a half-stroke; the only exceptions to this rule are the hover-flies using an inclined stroke plane (figures 10 and 11), where the middle of pronation is after the end of the upstroke. The latter half of rotation occurs while the wing accelerates into the following half-stroke. The wing is flexed across the chord during this period, which will be discussed in §3.6.3*b*. The two halves of pronation and supination last about the same length of time in general, although a more gradual beginning can be seen for the crane-flies (figures 7, 8) and the drone-fly (figure 12).

R. Å. Norberg (1972*b*) has demonstrated that the chordwise centre of mass for the wings

PHILOSOPHICAL TRANSACTIONS OF THE ROYAL SOCIETY B BIOLOGICAL SCIENCES

of several dragonfly species is posterior to the torsion axis except at the pterostigma, a thickened heavy spot close to the leading edge near the wing tip. With the centre of mass behind the torsion axis, the wing will tend to rotate as it decelerates and accelerates at the ends of half-strokes, a passive inertial response that will cause rotations in the correct directions. If the mass and torsion axes are too far apart, however, the rotations may be excessive and result in negative angles of attack at the beginning of half-strokes. This problem is analogous to the flutter of aeroplane wings and helicopter rotors, and Norberg suggests that the pterostigma may function as a dynamic mass balancer to prevent severe rotations. The pterostigma brings the centre of mass anterior to the torsion axis near the wing tip, and thus counteracts the usual inertial moments on more proximal regions. The position of the middle of pronation and supination on figures 6–16 supports this idea: if rotation was an inertial response to the wing flapping, the middle position would occur *after* the end of a half-stroke instead of before. Rotation must be the result of *active torsion* applied to the wing base, aided perhaps by the inertial response. The variable position of the middle of pronation for the hover-flies (figures 9–11) also suggests active control. It is likely that heavy areas close to the leading edge near the wing tip are responsible for an inertial balancing of the wing, and therefore regulate the relative proportions of active and passive rotation.

Pronation and supination are largely confined to the periods of acceleration and deceleration at the ends of half-strokes, and are approximately equal in duration. Each lasts 10–20 % of the cycle period: about 10 % for the crane-flies, 15 % for the ladybird and hover-fly, and 20 % for the drone-fly and the Hymenoptera. The wing rotates through a large angle during this time, typically 110°. The rotation carries the wing to an angle of attack some 10° less than that used on the following half-stroke, and the wing then *recoils* to the proper value. I suspect that it may be an elastic recoil, but can offer no proof. This was found at the end of pronation and supination for all of the insects and can be seen in the plates, particularly figure 18 (plate 1) for the crane-fly.

(*a*) *Angular velocity*. The angular velocity of rotation can be compared for different insects by using a non-dimensional form $\hat{\omega}$, equal to the mean angular velocity $\overline{\omega}$ during pronation and supination divided by the wingbeat frequency n. This represents the angle through which the wing would steadily rotate over a cycle period; values are given in table 2 for the sequences. These angles, about 10–21 rad, are of course much greater than the angle 2Φ that the wings flap through during a cycle, typically around 4 rad. For *Encarsia*, $\hat{\omega}$ is about 10 during the 'fling' at pronation (Weis-Fogh 1973), but values are less than 10 for *Schistocerca* (Jensen 1956) and *Phormia* (Nachtigall 1966, 1979) in fast forward flight.

In paper IV the velocity of the wing edges during rotation will be compared with that during flapping. A new dimensionless number is useful in that context: the mean rotational velocity $\overline{\omega}\bar{c}$ for the wing edge, based on the mean chord, divided by the mean flapping velocity of the wing tip, $\overline{U}_t = 2\Phi nR$. This ratio is simplified by using the relations above and in paper II, and its final form is $\hat{\omega}/\Phi\mathcal{R}$, where $\mathcal{R}$ is the aspect ratio of the wings. Values given in table 2 show that this ratio is close to unity for the insects. Thus the mean velocity of the wing edges during rotation is comparable with the mean flapping velocity for more distal regions of the wing.

This dimensionless number is somewhat similar to the Rossby number Ro encountered in flow situations combining steady rotation and linear streaming: $Ro = U/\omega a$, where U is the free-stream velocity and a is a characteristic length. In our case the rotational and linear velocities are both functions of time and are phase-shifted, so that the two conditions are not

directly comparable. Lugt & Ohring (1977) numerically investigated the viscous flow around an elliptic cylinder for *Ro* near unity. The flow patterns are striking and largely governed by the vorticity shed at the ends of the cylinder, a process strongly dependent on the rotational motion. The flow around rotating and flapping wings should be no less complicated: strong vortex-shedding from the leading and trailing edges during rapid rotations may influence the flow around the wing for the following half-stroke and violate the quasi-steady hypothesis (paper IV).

TABLE 2. MEAN NON-DIMENSIONAL ANGULAR VELOCITY OF ROTATION

(Mean values of $\hat{\omega}$ during pronation and supination are given, along with the ratio of mean rotational to flapping velocities for the wing edges. Insects from the selected film sequences are identified by their ID code from paper II.)

species	ID	$\hat{\omega}$/rad	$\hat{\omega}/\Phi R$
Coccinella 7-punctata	LB04	14.8	0.69
Tipula obsoleta	CF02	20.6	0.88
T. paludosa	CF04	17.5	0.74
Episyrphus balteatus	HF07	13.4	0.98
	HF08 (figure 10)	13.1	1.44
	HF08 (figure 11)	13.1	1.38
Eristalis tenax	DF01 (figure 12)	9.6	0.73
	DF01 (figure 13)	11.6	0.90
Apis mellifera	HB01	9.6	0.64
Bombus hortorum	BB04	9.6	0.70
B. lucorum	BB08	9.6	0.64

(*b*) *Profile flexion.* The wing does not rotate as a flat plate during the whole of pronation and supination; indeed, it exhibits strong changes in profile. As the wing decelerates at the end of a half-stroke and the angle of attack increases, corresponding to the onset of rotation, the wing untwists and any camber disappears. This indicates that rotation begins with the stiff anterior region of the wing, which includes the wing tip. At no time have I observed the flap or increased camber effects seen at the end of the downstroke for the locust (Jensen 1956) and *Drosophila* (Vogel 1967*a*). The wing continues to rotate like a flat plate until about the middle of pronation and supination, when a reversed curvature starts to develop. This curvature is fairly smooth and slight for the lacewing (figure 23; plates 17, 18 in Dalton 1975) and the nemopterid *Pterocroce*; smooth but more pronounced for the plume moth (figure 22; figures 1, 2 in R. Å. Norberg 1972*a*), *Manduca* and *Ephestia*; somewhat constrained to a localized flexion for the Diptera (figures 18–20; Nachtigall 1966, 1980; plate 66 in Dalton 1977; Wootton 1981) and the ladybird; and sharply defined for the Hymenoptera (figure 21; plate 24 in Dalton 1977; Wootton 1979). The curvature, or flexion, is usually greater for supination than pronation, and it largely disappears as the anterior wing area completes rotation and the posterior region catches up. By the time recoil occurs at the end of pronation and supination, the wing is nearly flat again.

This description of profile changes during rotation has been deliberately general, concentrating on the gross characteristics common to the insects. For a more detailed discussion of profile and flexing the reader is referred to the papers of Wootton (1979, 1981), who has begun

to address the functional interpretation of wing morphology. In particular, he draws attention to the significance of flexion lines in controlling wing deformations by allowing hingewise movements of whole areas of the wing. Two longitudinal flexion lines may act to localize alterations in the wing profile: the median flexion line and, more posteriorly, the claval furrow. The sharp flexing of the coupled hymenopteran wings during rotation occurs along the claval furrow, which is located just anterior to the first anal vein on the forewing. The bending observed for the Diptera and the ladybird appears to be somewhat confined to both flexion

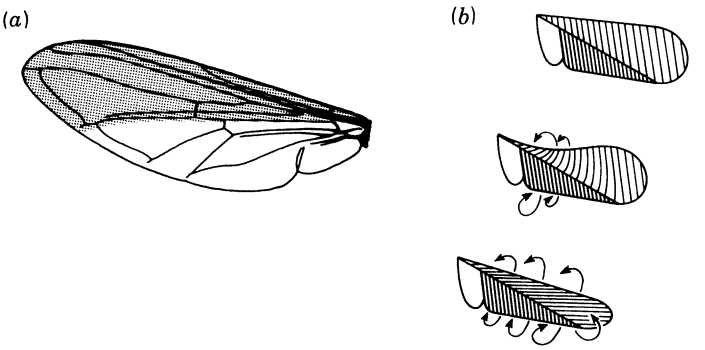

FIGURE 24. (*a*) Wing of the hover-fly *Episyrphus balteatus*, showing the two functionally distinct wing areas. The stiff anterior region is stippled. (*b*) The 'flip' motion proposed by Weis-Fogh, and the airflow it may generate. The alula is the posterior basal area, and is not involved in the flip. Progressing from top to bottom: the wing is initially flat; pronation causes a torsional wave in the anterior region moving towards the tip; pronation of the anterior area is complete before it occurs in the posterior region, giving rise to the flip profile (Weis-Fogh 1973).

lines, particularly the median one. For the other insects, however, the curvature during rotation seems quite smooth with little apparent discontinuity. This may be due to the relatively low resolution of the cine films, or else to a more restricted freedom of the flexion lines in these insects. Wootton (1981) also discusses the role of transverse flexion lines, which permit a ventral bending of the wing at the beginning of the upstroke for many insects. This bending can be seen in figure 23*l* for the forewing of *Chrysopa*, and it was also evident on some films of the tipulids and Hymenoptera. Again, the film resolution prevented more detailed observation.

A simplified model to explain the deformations during rotation consists of two more-or-less distinct wing areas separated by a longitudinal flexion line: a roughly triangular anterior region that includes the wing tip, usually stiff and reinforced by a concentration of veins, and the less supported posterior area. This generalization of wing morphology is identical to that proposed by Weis-Fogh (1973) for the hover-fly, shown in figure 24*a*. For four-winged insects with coupled wing pairs, the areas approximately correspond to the individual forewings and hindwings. The anterior wing area always appears to lead in rotation, reducing camber at the onset and then developing a reversed curvature in the latter half. When flexion is very localized, this produces a sharp angular movement between the two wing areas, the 'flip' motion suggested by Weis-Fogh for the hover-flies of the subfamily Syrphinae (figure 24*b*). This motion occurs to some extent for all of the filmed insects, as described above; the differences consist of the degree of localization for the flexing, and how much the anterior region leads the posterior (the angle between them). The Syrphinae, for which Weis-Fogh proposed this motion, *do not show an exceptional flip*: flexion is much the same as the other Diptera, and certainly less pronounced than the Hymenoptera.

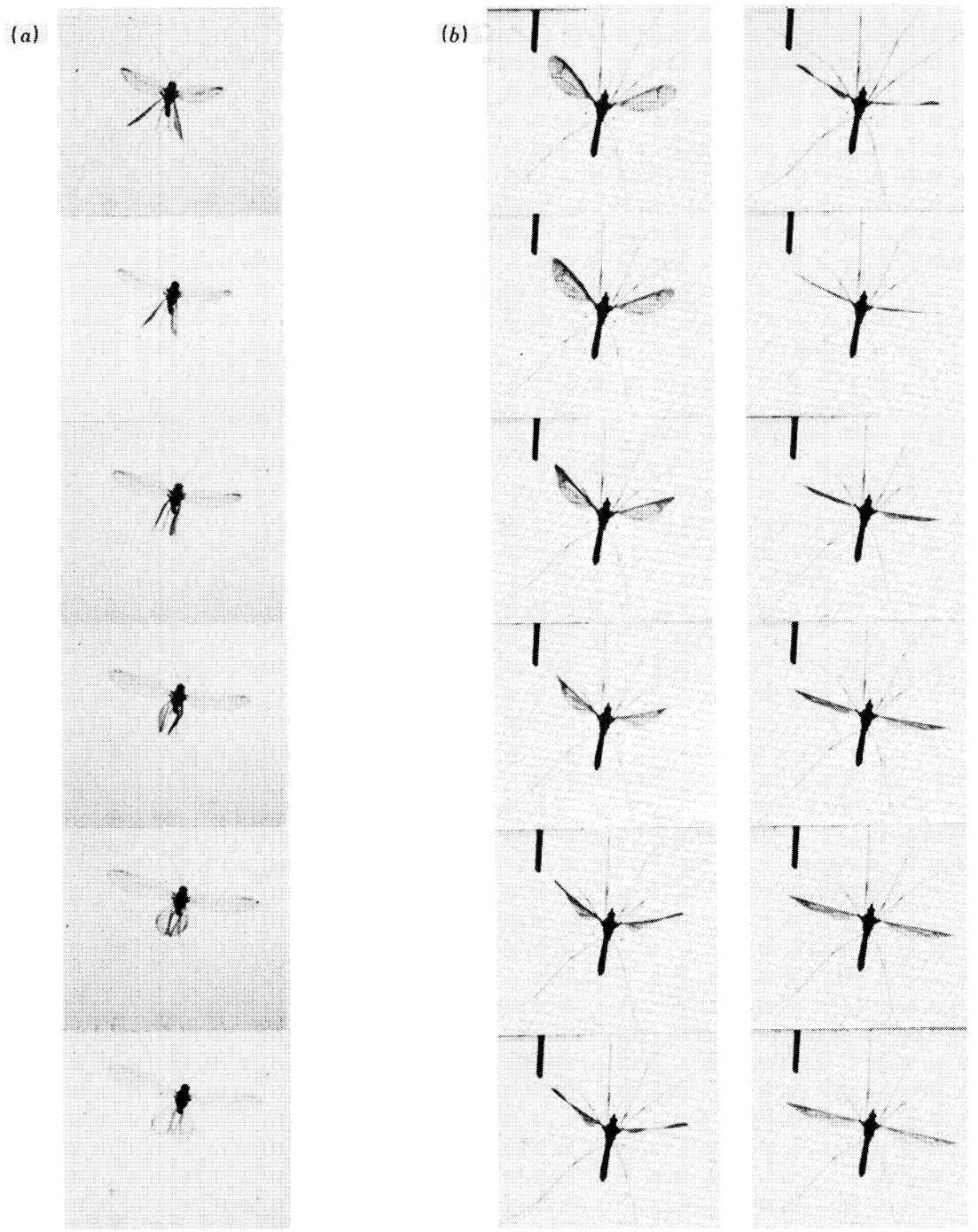

FIGURE 25. (*a*) A slight torsional wave moving towards the wing tip during supination of the hindwings of *Chrysopa*. (*b*) The latter half of supination for *Tipula obsoleta*. The anterior wing area rotates first, producing a torsional wave passing through the posterior region towards the wing base. Elastic recoil of the angle of attack is evident at the end of supination.

(*Facing p.* 71)

PHILOSOPHICAL TRANSACTIONS OF THE ROYAL SOCIETY B BIOLOGICAL SCIENCES

The flip has a double meaning, referring also to a postulated aerodynamic mechanism based on the wing flexing. Weis-Fogh (1973) concluded that quasi-steady aerodynamics could not explain the hovering of Syrphinae with an inclined stroke plane, and suggested that the airflow created by the flip motion would generate a wing circulation, and hence lift, greater than the conventional value. If this flip mechanism does explain the flight of hover-flies, then it must also apply to other insects that have a similar flip motion. But here is the rub: Weis-Fogh concluded in the same paper that these insects (*Eristalis*, *Tipula* and the Hymenoptera) fly according to quasi-steady aerodynamics. This contradiction will be considered in more detail in papers IV and VI.

(*c*) *Torsional waves*. With particular reference to the flip motion in hover-flies, Weis-Fogh (1973) suggested that active rotation at the wing base results in torsional waves moving towards the tip. On the assumption that the propagation of these waves is mediated by elastic and inertial forces only, he calculated that their velocity through stiff cuticle is about 51 m s^{-1}, using the simple formula for a *circular rod* of material: the wave velocity is likely to be much lower, however, when aerodynamic damping is important and the cross-section is not circular (K. E. Machin, personal communication). The time required for Weis-Fogh's wave to reach the wing tip is 2–3 % of the cycle period, and is a significant fraction of the total rotation time for some insects. Thus the rotation of distal wing regions should lag behind more proximal ones, a phenomenon that Weis-Fogh called 'delayed elasticity'. (This is an unfortunate misnomer, since the elasticity is in no sense 'delayed': the process is a simple torsional wave). As shown in figure 24*b*, Weis-Fogh proposed that the torsional deformation would propagate along the stiff anterior wing area first. The softer posterior region should have a lower shear modulus, which results in a slower wave speed; its rotation would lag behind the anterior area, producing the flip profile in the meantime. The flip motion in figure 24*b* shows this intermediate profile, before the posterior area rotates significantly.

A slight torsional wave moving towards the wing tip was noticed during supination of the hindwings of *Chrysopa*, and is illustrated in figure 25*a*, plate 7. Both wing areas are relatively soft, with a low wave velocity, and the wave seems to propagate through them at nearly the same speed: little chordwise curvature is evident, and a sharp flip profile is absent. For the other insects, the stiff anterior wing area rotates as a unit with *no* visible deformations. It must be remembered that torsional waves result from the angular accelerations in rotation, not the angular velocity. Deformations produced by the gradual change in the angle of attack at the beginning of rotation must be small in amplitude, and hence do not contribute significantly to the angle of attack at a particular spanwise station. Torsional waves could not be detected in the softer posterior wing area either, except for the ladybird,the Diptera and the Lepidoptera. For these insects *the wave progresses towards the wing base* during the latter half of rotation, which is the opposite direction to that suggested by Weis-Fogh. This wave is seen in figure 25*b* for supination in the crane-fly, where it is greatly pronounced. The sequence starts at about the middle of supination: the anterior area, including the wing tip, rotates first; the posterior region then rotates in a wave passing from tip to base; and the entire wing recoils to the angle of attack for the following upstroke. Wootton (1981) also describes this phenomenon for tipulids and some dragonflies (Odonata). The flexion lines separating the wing areas generally run obliquely to the longitudinal wing axis, curving towards the trailing edge (Wootton 1981). Rotation of the anterior wing area will generate a moment across the distal posterior region because of this, which may explain the origin of the wave.

PHILOSOPHICAL TRANSACTIONS OF THE ROYAL SOCIETY B BIOLOGICAL SCIENCES

3.7 *Wing interference*

At either end of the wingbeat, particularly the dorsal one, the left and right wings may be in close proximity. They will influence the airflow around each other then, producing an aerodynamic interference that may be beneficial.

3.7.1 *The clap and fling*

The most striking example of beneficial interference is the 'clap and fling' described by Weis-Fogh (1973) for the small wasp *Encarsia*. At the end of the upstroke the coupled wings rotate, their leading edges touch, and the wings clap together. The wings remain clapped for a surprisingly long time, about 20–25% of the cycle period, which may correspond to elastic storage of the high mechanical energy needed for the subsequent 'fling' motion (Ellington 1975). After the clap the wings pronate with the trailing edges still in contact, and fling open rather like a book. Weis-Fogh proposed that the airflow caused by the fling creates a circulation around each wing, a circulation that is *independent* of quasi-steady considerations. This unsteady flight mechanism enables *Encarsia* to generate sufficient circulatory lift even at very low Reynolds numbers, and will be discussed in detail in paper IV.

The clap and fling occurs in all small insects that have been studied: *Drosophila melanogaster* and *Thrips physapus* (my films), *D. virilis* (plate 1 in Vogel 1967*a*) and the greenhouse white-fly *Trialeurodes vaporariorum* (Weis-Fogh 1975). It is also found in some larger insects. Cooter & Baker (1977) report it for the hindwings of *Locusta migratoria* in climbing flight, and it is a prominent feature for many moths and butterflies, usually visible to the naked eye. My films reveal a clap and fling for the Large Cabbage White butterfly *Pieris brassicae* (also found by Weis-Fogh 1975), the plume moth *Emmelina* (figure 22) and the flour moth *Ephestia*. Chance (1975) found it in the red-backed cutworm moth *Euxoa ochragaster*, and it is evident in still photographs of various other Lepidoptera (figure 2.D3 in R. Å. Norberg 1972*a*; plate 21 in Dalton 1975; plates 28 and 38 in Dalton 1977).

The prolonged clap of *Encarsia* is exceptional and cannot be seen in films of the other insects. For them, the rotational motion of each wing during the clap and fling is much the same as normal pronation. Thus the clap and fling does not involve a significant change in the basic wingbeat pattern except for the fact that the wings meet dorsally. The longitudinal wing axes tend to rise slightly above the stroke plane as the wings clap together, which can be seen in figure 22 for *Emmelina*. This vertical movement is most pronounced for *Emmelina* and *Pieris*, where it is equal to about 15°; for the other insects it is less than 10°. The fling commences at the top of this vertical excursion, and there is a slight downward motion during the fling and subsequent separation of the wings.

3.7.2. *The peel*

Weis-Fogh described the fling as a rigid rotation of the wing surfaces about their trailing edges, and Lighthill (1973) analysed the fluid mechanics of this motion. The fling is more aptly described as a *peel* in the Lepidoptera and *Drosophila*, however, and is rather like pulling two pieces of paper apart by their leading edges. The wings are curved along their chords, and the point of separation moves smoothly from the leading to trailing edges during the peel (figure 22*b–d*). The wing curvature may just be that normally observed in pronation, enhanced to some extent by elastic deformation under the aerodynamic and inertial loads. The high

PHILOSOPHICAL TRANSACTIONS OF THE ROYAL SOCIETY B BIOLOGICAL SCIENCES

resolution still photographs of other authors mentioned above show the peel with great clarity. Although it may seem an almost trivial kinematic modification to the fling, the aerodynamic implications of the peel are quite important. These will be discussed in paper IV, where it will be shown that the peel is substantially more effective than the fling in creating a circulation around the wings. The tiny four-winged insects probably do not perform a rigid rotation of the entire wing surface during a fling either. These insects cannot peel apart their relatively stiff wings, but they may do a *double fling*. Because the forewings led the hindwings in the cycle, the fling should be a two-stage process: the forewings fling apart first, followed by the hindwings. It is very difficult to verify this on the films of *Encarsia* and *Thrips*, but a few tantalizing frames suggest that it is true. If that is the case, then the double fling may provide the small insects with some of the benefits of the smooth peeling motion.

3.7.3. *A continuous spectrum*

Except for *Drosophila*, the small insects are the only ones that always use a complete clap and fling. The remaining insects vary $\phi_{\max}$ slightly during manoeuvres, often resulting in a *partial* or *near* clap and fling. There is a continuous spectrum of motions, all based on the normal pronation, corresponding to the distance separating the wing pairs: in the full clap and fling the wings are momentarily in contact along the entire chord, in the partial clap and fling this contact is restricted to a posterior region of the chord, and in the near clap and fling the wings are close together but do not touch. The separation distance varies along the wing as a function of the chord and the angle between the longitudinal wing axes. Thus a partial clap and fling at the wing base can gradually change into a near clap and fling at the tip. This was the greatest separation observed for the Lepidoptera during pronation: a partial clap and fling confined to the most basal wing region. An intermediate motion was more commonly noted, though, with the wings touching at least along the trailing edges for much of their length. A near clap and fling was sometimes seen for *Ephestia* and *Pieris* during supination as well: the wings were separated by less than 0.2 of the mean chord $\bar{c}$ along most of their length. Normally the wings were well clear of each other during supination.

Many other insects also work their way along this spectrum, although few achieve a complete clap and fling. Some general comments will be made about the wing motion, however, before delving into specifics. As already noted, the wing chords are parallel to each other and perpendicular to the stroke plane at the middle of rotation. The separation between the leading edges is smallest at this point in the cycle. As rotation continues the trailing edges come closer together, reaching a minimum separation about two-thirds of the way through rotation, and then move apart as the wings accelerate into the next half-stroke. The *axis of rotation* should lie somewhere in the anterior half of the wing chord to generate this motion: the residual flapping movement when the middle of rotation occurs just before the end of a half-stroke is insufficient to explain it. Because the wings rotate in this manner, the clap is missing from a partial clap and fling. Contact is made after the middle of rotation, when the wings are flinging open, and is limited to more posterior areas of the chord. For the near clap and fling, we can use the minimum distance between the trailing edges at the middle of the wing as a measure of wing separation.

The lacewing is the most interesting example from the filmed insects, demonstrating the greatest range with its uncoupled wing pairs. In figure 23 there is a very small gap between the forewings in pronation, and between the hindwings in pronation and supination. (The

forewings, however, are well apart in supination.) The separation for these motions varied on different films: it increased to about $\frac{1}{2}\bar{c}$ for the near clap and fling, decreased until the trailing edges just touched in a partial clap and fling, and anything in between. A more comprehensive partial fling was sometimes found for the hindwings in pronation. The wing motions of the other neuropteran *Pterocroce* were also quite variable. The trailing edges were usually separated by $\frac{1}{2}\bar{c}-\frac{1}{2}\bar{c}$ in pronation but were well clear in supination. Unlike the lacewing, a complete dorsal clap and fling was noted a few times. The ladybird uses a near (about $\frac{1}{4}\bar{c}$) to partial clap and fling during pronation, and only a near one in supination (greater than about $\frac{1}{4}\bar{c}$). The tipulids also use near (figure 18) to partial motions in pronations, with the trailing edges typically separated by $\frac{1}{4}\bar{c}-\frac{3}{4}\bar{c}$, but the wings are clear in supination. The Hymenoptera do a near double fling in pronation because of the sharp wing flexing (figure 21): $\phi_{\max}$ is relatively constant, and the separation is about $\frac{3}{4}\bar{c}$. Finally, the wings are always well separated for *Episyrphus* and *Eristalis*.

To judge from the films, the wing separation generally seems to change with the net lift generated: in manoeuvres demanding greater lift the wings tend to come closer together, and vice versa. This may simply reflect control of the net lift via the stroke angle Φ. The difference in $\phi_{\max}$ between a partial and near clap and fling may be but a few degrees, however, and the change in lift due to the altered stroke angle would be small. Perhaps the wing separation can provide a fine control over the circulation created around the wings, and hence the amount of lift produced. If the partial clap and fling is somewhat less effective than the complete one in generating a circulation, and the near clap and fling even less so, then all of the insects using these motions may rely on a variant of the unsteady fling mechanism, controlling the circulation and net lift by subtle changes in the wing separation. This suggestion will be further investigated in paper IV.

4. Appendix

Errors in the film analysis procedure

The second perspective approximation, that all projection rays from the object are parallel to the *xy* plane, permits a horizontal reference plane to be defined for the insect coordinate system, and will be discussed first. Consider the line passing through the optical centre and the centre of the object sphere in figure 2. Points that lie in the plane defined by this line and the horizontal line $\hat{z} = \hat{z}_0$ project onto that horizontal line in the object plane, and onto the corresponding line in the image plane. I have assumed, however, that these points lie in a true horizontal plane perpendicular to the object and image planes: thus the assumed horizontal plane is actually tilted by a small angle with respect to the true horizontal because of perspective. The maximum tilt occurs at the extreme values of $\hat{z}_0$ when $\hat{y}_0$ is zero, and can be estimated in radians by $(0.34\ \hat{W}-1)/\hat{S}$. For values of 8 and 40 for $\hat{W}$ and $\hat{S}$ respectively, the maximum tilt is only 2.5°. $\hat{S}$ was about 15 for Weis-Fogh's (1973) films of *Manduca* (G. G. Runnalls, personal communication), giving a maximum tilt of 7° for them.

Although the image wing length results from a perspective projection, the spatial angles of the wing are reconstructed as if the image was a parallel projection. The errors introduced by this approximation may be investigated initially by considering an object sphere located on the optical axis. Because of the axial symmetry of perspective this case then reduces to an object circle in the *xy* plane, as shown in figure 26*a*: the distance $\hat{S}$ is greatly reduced to exaggerate the differences between perspective and parallel projections. The wing position is defined by the angle γ between it and the line joining the centre of the sphere to $\hat{S}$. The perspective wing

PHILOSOPHICAL TRANSACTIONS OF THE ROYAL SOCIETY B BIOLOGICAL SCIENCES

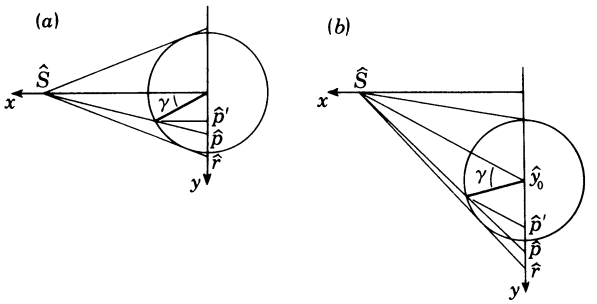

FIGURE 26. Comparison between a perspective wing tip projection $\hat{p}$ and a parallel projection $\hat{p}'$. The object circle lies on the optical axis in (*a*), off it in (*b*).

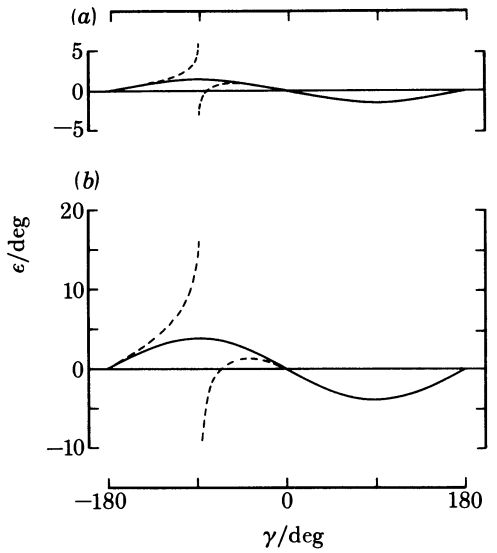

FIGURE 27 The error angle ϵ arising from the parallel projection assumption, is plotted against wing position γ. In (*a*) $\hat{S} = 40$; in (*b*) $\hat{S} = 15$.

tip projection onto the object plane is denoted by $\hat{p}$, and that which would be obtained by a parallel projection is indicated by $\hat{p}'$. The maximum projected wing length for the perspective case $\hat{r}$ is greater than unity, which is the value $\hat{r}'$ for a parallel projection. If the wing image was actually a parallel projection, then the angle γ could be calculated exactly by

$$\gamma = \sin^{-1}(\hat{p}'/\hat{r}'). \tag{26}$$

Because the image wing length $\hat{p}$ and its maximum value $\hat{r}$ are the result of perspective projections, however, the angle γ_p estimated from them will be slightly incorrect:

$$\gamma_p = \sin^{-1}(\hat{p}/\hat{r}). \tag{27}$$

An error angle ϵ, equal to the difference between the true angle and that estimated from the assumption, is given by the solid lines in figures 27*a*, *b*, for $\hat{S}$ equal to 40 and 15. The maximum error occurs at the two values of γ where the perspective rays are tangential to the circle and the projected wing length is greatest, and is only 1.4° for $\hat{S}$ equal to 40 and 3.8° for the smaller value. It may be calculated for any similar optical system by

$$\epsilon_{max} = \cos^{-1}[(\hat{S}^2 - 1)/\hat{S}^2]^{\frac{1}{2}}. \tag{28}$$

When the object circle is off the optical axis, ϵ is not very different except for values of γ around the tangent point nearest to the x axis. The image wing length at this point is less than the maximum $\hat{r}$ at the other tangent, as shown in figure 26*b*. The estimated angle γ_p must be double-valued at the near-tangent point, therefore, and the interval between the two values is lost. This effect is indicated by the dashed lines in figures 27*a*, *b* for the worst off-axis case, $\hat{y}_0 = 3$, and it is clear that errors for small values of $\hat{S}$ can indeed be large. If the angles on either side of the ray passing through the centre of the circle are reconstructed with the maximum projected wing length on the *corresponding side*, however, the error angle is very close to the on-axis case over the entire circle. The kinematics are only determined for one wing in general, so the problem of treating two tangents will rarely arise.

An inherent problem of projection analysis is that the reconstructed angles are sensitive to small measurement errors when the wing is close to maximum projection. An inaccuracy of only 1 % in the measured wing length can lead to errors of $\pm 8°$ when the wing is parallel to the object plane. Fortunately, the effect is sharply peaked at maximum projection: the error falls to $\pm 3°$ for positions 10° on either side of the object plane, to less than $\pm 2°$ for positions of 20°, and to less than $\pm 1°$ for the remaining range. It is unlikely, however, that one cine frame will show the true maximum projection because of the limited number of frames per wingbeat. For a reasonable filming speed, about 30 frames per wingbeat, it is probable that one frame will show the wing within 10° of maximum projection. Apart from any measurement inaccuracy, the error will be large for this frame if it is chosen to represent the 'true' maximum wing length. By the next frame, however, the error from using this length will fall to about 2°. Thus the problems of measurement inaccuracies and finite filming speed are very similar, and indicate that the wing position in the frame showing the maximum observed wing length must be regarded as unreliable. This wing length may be used as the 'true' maximum projection for other frames, though, and the error of the reconstructed angles will typically be less than 2°.

Finally, I wish to comment on the implicit assumption that the wing is rigid along its longitudinal axis; that is, the length from base to tip must be constant for the projection analysis. A small bending along the axis does not significantly alter this length, and changes in length up to about 1 % can be tolerated without serious errors. The only effect is that the calculated position of the wing tip lags slightly behind more proximal wing regions. If the bending is too large, however, the analysis is not valid. This was the case for *Ephestia*, where extreme bending at the end of the downstroke and beginning of the upstroke caused the distance from wing base to tip to decrease by about 4 %.

I am grateful to Mr G. G. Runnalls, whose expertise in high-speed cinematography made this work possible. I also thank Mr D. J. Tyler for building the digitizer, Professor G. K. Batchelor for laboratory space and computing facilities in the Department of Applied Mathematics and Theoretical Physics, Mr J. H. Davidson for computing assistance, and Dr K. E. Machin for discussions and comments on the manuscript. The Winston Churchill Foundation and the Science and Engineering Research Council provided financial support.

References

Baker, P. S. & Cooter, R. J. 1979 The natural flight of the migratory locust, *Locusta migratoria* L. I. Wing movements. *J. comp. Physiol.* **131** 79–87.

Bilo, D. 1971 Flugbiophysik von Kleinvögeln I. Kinematik und Aerodynamik des Flügelabschlages beim Haussperling (*Passer domesticus* L.). *Z. vergl. Physiol.* **71**, 382–454.

PHILOSOPHICAL TRANSACTIONS OF THE ROYAL SOCIETY B BIOLOGICAL SCIENCES

Bilo, D. 1972 Flugbiophysik von Kleinvögeln II. Kinematik und Aerodynamik des Flügelaufschlages beim Haussperling (*Passer domesticus* L.). *Z. vergl. Physiol.* **76**, 426–437.
Burton, A. J. & Sandeman, D. C. 1961 The lift provided by the elytra of the Rhinoceros beetle, *Oryctes boas* Fabr. *S. Afr. J. Sci.* **57**, 107–109.
Chance, M. A. C. 1975 Air flow and the flight of a noctuid moth. In *Swimming and flying in Nature* (ed. T. Y. Wu, C. J. Brokaw & C. Brennen), vol. 2, pp. 829–843. New York: Plenum Press.
Cooter, R. J. & Baker, P. S. 1977 Weis-Fogh clap and fling mechanism in *Locusta*. *Nature, Lond.* **269**, 53–54.
Dalton, S. 1975 *Borne on the wind.* London: Chatto & Windus.
Dalton, S. 1977 *The miracle of flight.* London: Sampson Low.
David, C. T. 1978 The relationship between body angle and flight speed in free-flying *Drosophila*. *Physiol. Ent.* **3**, 191–195.
David, C. T. 1979 Optomotor control of speed and height by free-flying *Drosophila*. *J. exp. Biol.* **82**, 389–392.
David, C. T. 1982 Compensation for height in the control of groundspeed by *Drosophila* in a new, 'Barber's Pole' wind tunnel. *J. comp. Physiol.* **147**, 485–493.
Ellington, C. P. 1975 Non-steady-state aerodynamics of the flight of *Encarsia formosa*. In *Swimming and flying in Nature* (ed. T. Y. Wu, C. J. Brokaw & C. Brennen), vol. 2, pp. 783–796. New York: Plenum Press.
Esch, H., Nachtigall, W. & Kogge, S. N. 1975 Correlations between aerodynamic output, electrical activity in the indirect flight muscles and wing positions of bees flying in a servomechanically controlled wind tunnel. *J. comp. Physiol.* **100**, 147–159.
Götz, K. G. 1968 Flight control in *Drosophila* by visual control of motion. *Kybernetik* **4**, 199–208.
Greenewalt, C. H. 1960 *Hummingbirds.* New York: Doubleday.
Greenewalt, C. H. 1962 Dimensional relationships for flying animals. *Smithson. misc. Collns* **144**(2), 1–46.
Greenewalt, C. H. 1975 The flight of birds. *Trans. Am. phil. Soc.* **65**(4), 1–67.
Hertel, H. 1966 *Structure, form, movement.* New York: Reinhold.
Hollick, F. S. J. 1940 The flight of the dipterous fly *Muscina stabulans* Fallen. *Phil. Trans. R. Soc. Lond.* B **230**, 357–390.
Jensen, M. 1956 Biology and physics of locust flight. III. The aerodynamics of locust flight. *Phil. Trans. R. Soc. Lond.* B **239**, 511–552.
Lighthill, M. J. 1973 On the Weis–Fogh mechanism of lift generation. *J. Fluid Mech.* **60**, 1–17.
Lugt, H. J. & Ohring, S. 1977 Rotating elliptic cylinders in a viscous fluid at rest or in a parallel stream. *J. Fluid Mech.* **79**, 127–156.
Magnan, A. 1934 *La locomotion chez les animaux I. Le vol des insectes.* Paris: Hermann et Cie.
Marey, E. J. 1873 *La machine animale.* Paris: G. Ballilière.
Nachtigall, W. 1966 Die Kinematik der Schlagflügelbewegungen von Dipteren. Methodische und Analytische Grundlagen zur Biophysik des Insektenflugs. *Z. vergl. Physiol.* **52**, 155–211.
Nachtigall, W. 1973 Investigation of wing movements and the generation of aerodynamic forces in flying Diptera. In *Comparative physiology* (ed. L. Bolis, K. Schmidt-Nielsen & S. H. P. Maddrell), pp. 77–79. Amsterdam: North-Holland.
Nachtigall, W. 1979 Rasche Richtungsänderungen und Torsionen schwingender Fliegenflügel und Hypothesen über zugeordnete instationäre Strömungseffekte. *J. comp. Physiol.* **133**, 351–355.
Nachtigall, W. 1980 Rasche Bewegungsänderungen bei der Flügelschwingung von Fliegen und ihre mögliche Bedeutung für instationäre Luftkrafterzeugung. In *Instationäre Effeckte an schwingenden Tierflügeln* (ed. W. Nachtigall), pp. 115–129. Weisbaden: Franz Steiner.
Nachtigall, W. 1981 Insect flight aerodynamics. In *Locomotion and energetics in arthropods* (eds. C. F. Herreid & C. R. Fourtner), pp. 127–162. New York: Plenum Press.
Nachtigall, W., Widmann, R. & Renner, M. 1971 Über den 'ortsfesten' freien Flug von Bienen in einem Saugkanal. *Apidologie* **2**, 271–282.
Neuhaus, W. & Wohlgemuth, R. 1960 Über das Fächeln der Bienen und dessen Verhaltnis zum Fliegen. *Z. vergl. Physiol.* **43**, 615–641.
Norberg, R. Å. 1972*a* Flight characteristics of two plume moths, *Alucita pentadactyla* L. and *Orneodes hexadactyla* L. (Microlepidoptera). *Zool. Scr.* **1**, 241–246.
Norberg, R. Å. 1972*b* The pterostigma of insect wings an inertial regulator of wing pitch. *J. comp. Physiol.* **81**, 9–22.
Oehme, H. & Kitzler, U. 1974 Untersuchungen zur Flugbiophysik und Flugphysiologie der Vögel. I. Über die Kinematik des Flügelschlages beim unbeschleunigter Horizontalflug. *Zool. Jb.* **78**, 461–512.
Pfau, H. K. 1977 Zur Morphologie und Funktion des Vorderflügels und Vorderflügelgelgelenks von *Locusta migratoria* L. In *The Physiology of movement; biomechanics* (ed. W. Nachtigall), pp. 347–352. Stuttgart: Fischer.
Pfau, H. K. & Nachtigall, W. 1981 Der Vorderflügel grosser Heuschrecken als Luftkrafterzeuger. II Zusammenspiel von Muskeln und Gelenkmechanik bei der Einstellung der Flügelgeometrie. *J. comp. Physiol.* **142**, 135–140.
Stellwaag, F. 1914 Der Flug der Lamellicornier. *Z. wiss. Zool.* **108**, 359–429.
Stellwaag, F. 1916 Wie steuern die Insekten während des Fluges? *Biol. Zbl.* **36**, 30–44.
Stolpe, M. & Zimmer, K. 1939 Der Schwirrflug des Kolibri im Zeitlupenfilm. *J. Orn., Lpz.* **87**, 136–155.
Vogel, S. 1966 Flight in *Drosophila*. I. Flight performance of tethered flies. *J. exp. Biol.* **44**, 567–578.
Vogel, S. 1967*a* Flight in *Drosophila*. II. Variations in stroke parameters and wing contour. *J. exp. Biol.* **46**, 383–392.

PHILOSOPHICAL TRANSACTIONS OF THE ROYAL SOCIETY B BIOLOGICAL SCIENCES

Vogel, S. 1967*b* Flight in *Drosophila*. III. Aerodynamic characterisics of fly wings and wing models. *J. exp. Biol.* **46**, 431–443.
Walker, G. T. 1925 The flapping flight of birds. *Jl R. aeronaut. Soc.* **29**, 590–594.
Weis-Fogh, T. 1956 Biology and physics of locust flight. II. Flight performance of the desert locust (*Schistocerca gregaria*). *Phil. Trans. R. Soc. Lond.* B **239**, 459–510.
Weis-Fogh, T. 1972 Energetics of hovering flight in hummingbirds and in Drosophila. *J. exp. Biol.* **56**, 79–104.
Weis-Fogh, T. 1973 Quick estimates of flight fitness in hovering animals, including novel mechanisms for lift production. *J. exp. Biol.* **59**, 169–230.
Weis-Fogh, T. 1975 Flapping flight and power in birds and insects, conventional and novel mechanisms. In *Swimming and flying in Nature* (ed. T. Y. Wu, C. J. Brokaw & C. Brennen), vol. 2, pp. 729–762. New York: Plenum Press.
Wood, J. 1970 A study of the instantaneous air velocities in a plane behind the wings of certain Diptera flying in a wind tunnel. *J. exp. Biol.* **52**, 17–25.
Wootton, R. J. 1979 Function, homology and terminology in insect wings. *Syst. Ent.* **4**, 81–93.
Wootton, R. J. 1981 Support and deformability in insect wings. *J. Zool.* **193**, 447–468.
Zarnack, W. 1972 Flugbiophysik der Wanderheuschrecke (*Locusta migratoria* L.). I. Die Bewegungen der Vorderflügel. *J. comp. Physiol.* **78**, 356–395.

PHILOSOPHICAL TRANSACTIONS OF THE ROYAL SOCIETY B BIOLOGICAL SCIENCES

FIGURE 18. The sequence for the crane-fly *Tipula obsoleta*, used in figure 7. Alternate frames are shown.

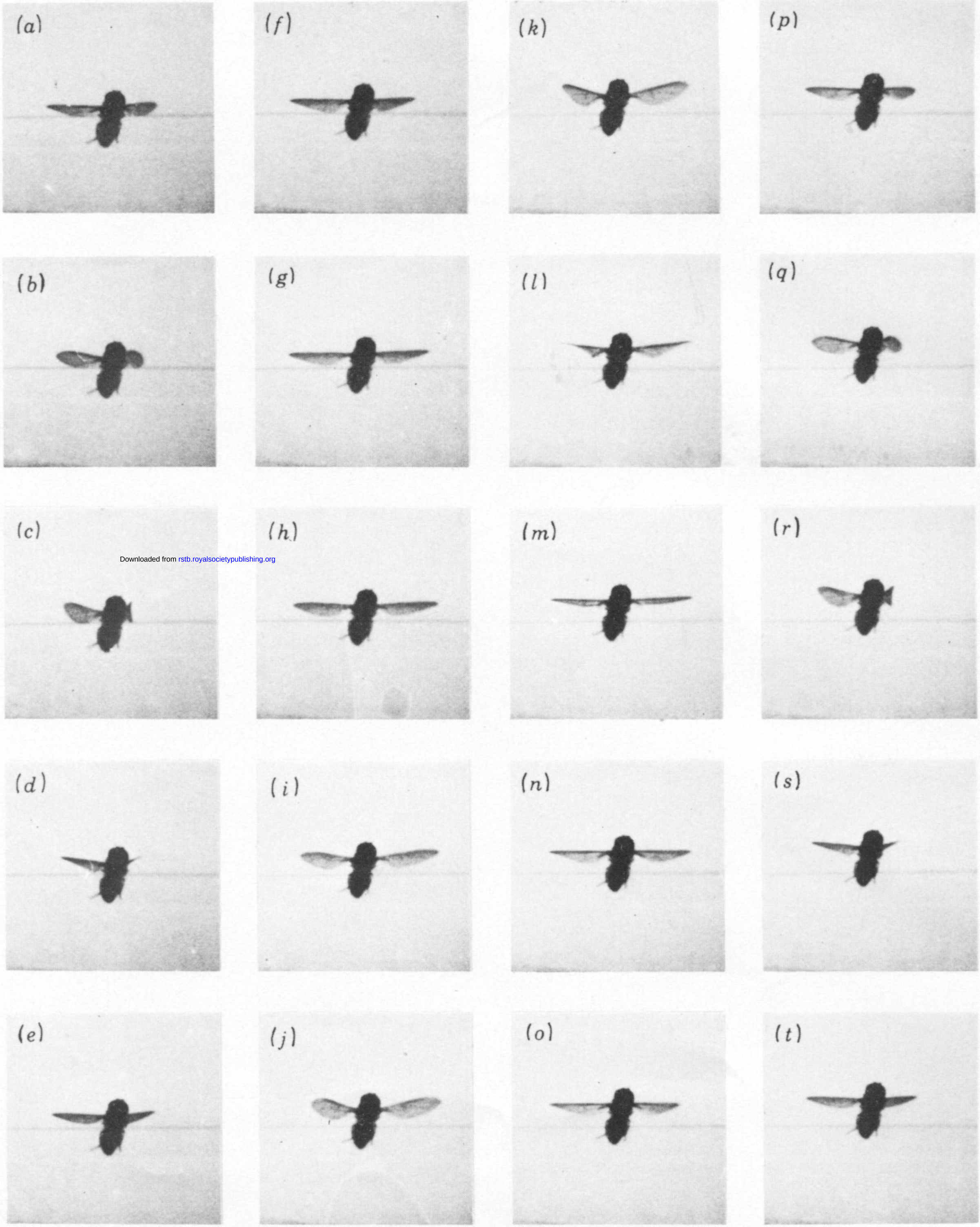

PHILOSOPHICAL TRANSACTIONS OF THE ROYAL SOCIETY B BIOLOGICAL SCIENCES

FIGURE 19. The sequence for the hover-fly *Episyrphus balteatus*, used in figure 9. Alternate frames are shown.

PHILOSOPHICAL TRANSACTIONS OF THE ROYAL SOCIETY B BIOLOGICAL SCIENCES

IGURE 20. The sequence for the drone-fly *Eristalis tenax*, used in figure 12. Alternative frames are shown.

PHILOSOPHICAL TRANSACTIONS OF THE ROYAL SOCIETY B BIOLOGICAL SCIENCES

FIGURE 21. The sequence for the bumble bee *Bombus lucorum*, used in figure 16.

PHILOSOPHICAL TRANSACTIONS OF THE ROYAL SOCIETY B BIOLOGICAL SCIENCES

FIGURE 22. The wingbeat of the plume moth (PM01) *Emmelina monodactylus* in decelerating forward flight. Kinematic parameters: $\hat{V} = 1.42$, $\xi = -3°$, $\eta = 12°$, $\beta = 9°$, $\overline{\chi} = 59°$, $\Phi = 168°$, $\overline{\phi} = 13°$, $n = 32.9$ Hz, $d/u = 1.42$. Alternate frames are shown.

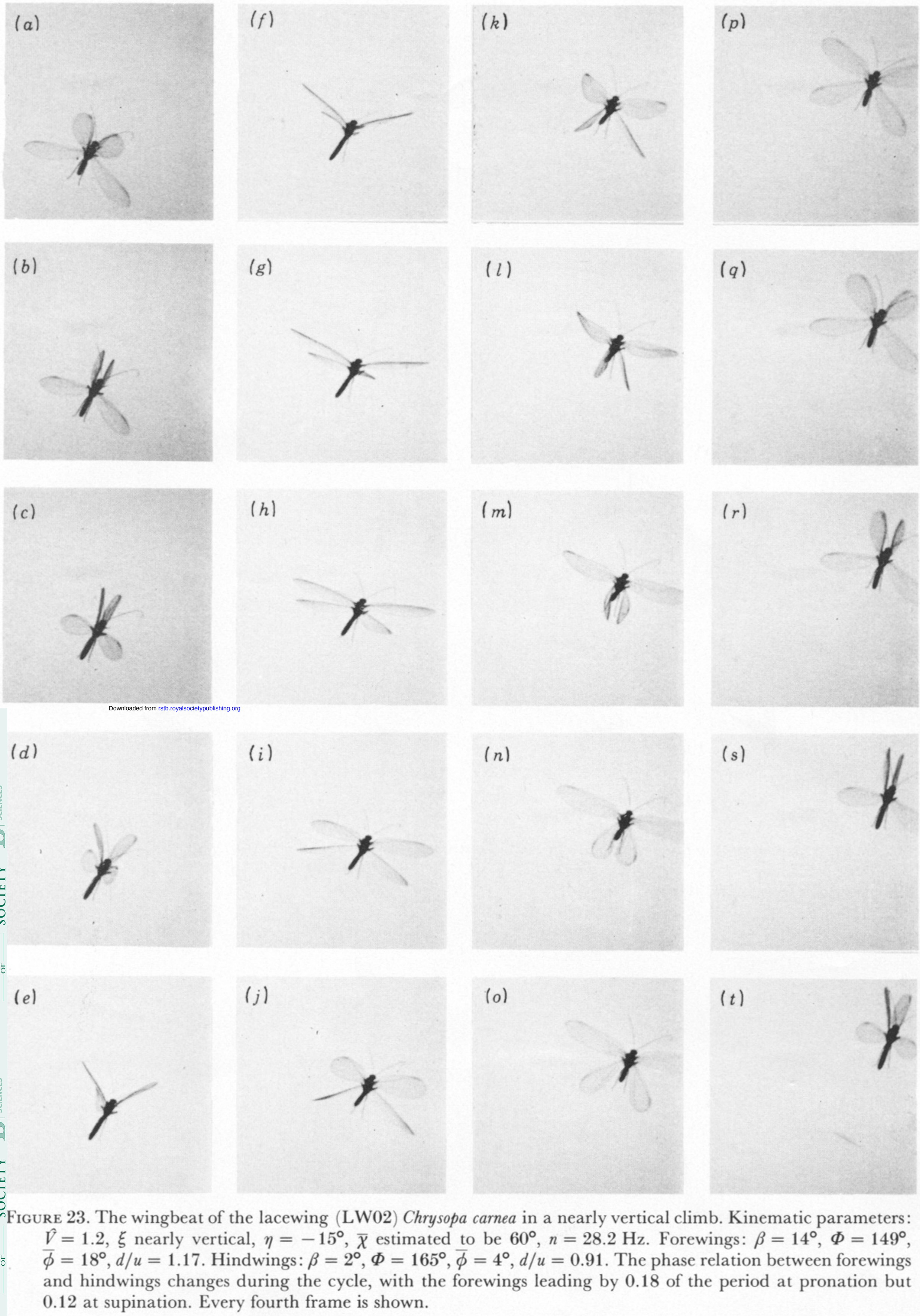

FIGURE 23. The wingbeat of the lacewing (LW02) *Chrysopa carnea* in a nearly vertical climb. Kinematic parameters: $\hat{V} = 1.2$, ξ nearly vertical, $\eta = -15°$, $\overline{\chi}$ estimated to be 60°, $n = 28.2$ Hz. Forewings: $\beta = 14°$, $\Phi = 149°$, $\overline{\phi} = 18°$, $d/u = 1.17$. Hindwings: $\beta = 2°$, $\Phi = 165°$, $\overline{\phi} = 4°$, $d/u = 0.91$. The phase relation between forewings and hindwings changes during the cycle, with the forewings leading by 0.18 of the period at pronation but 0.12 at supination. Every fourth frame is shown.

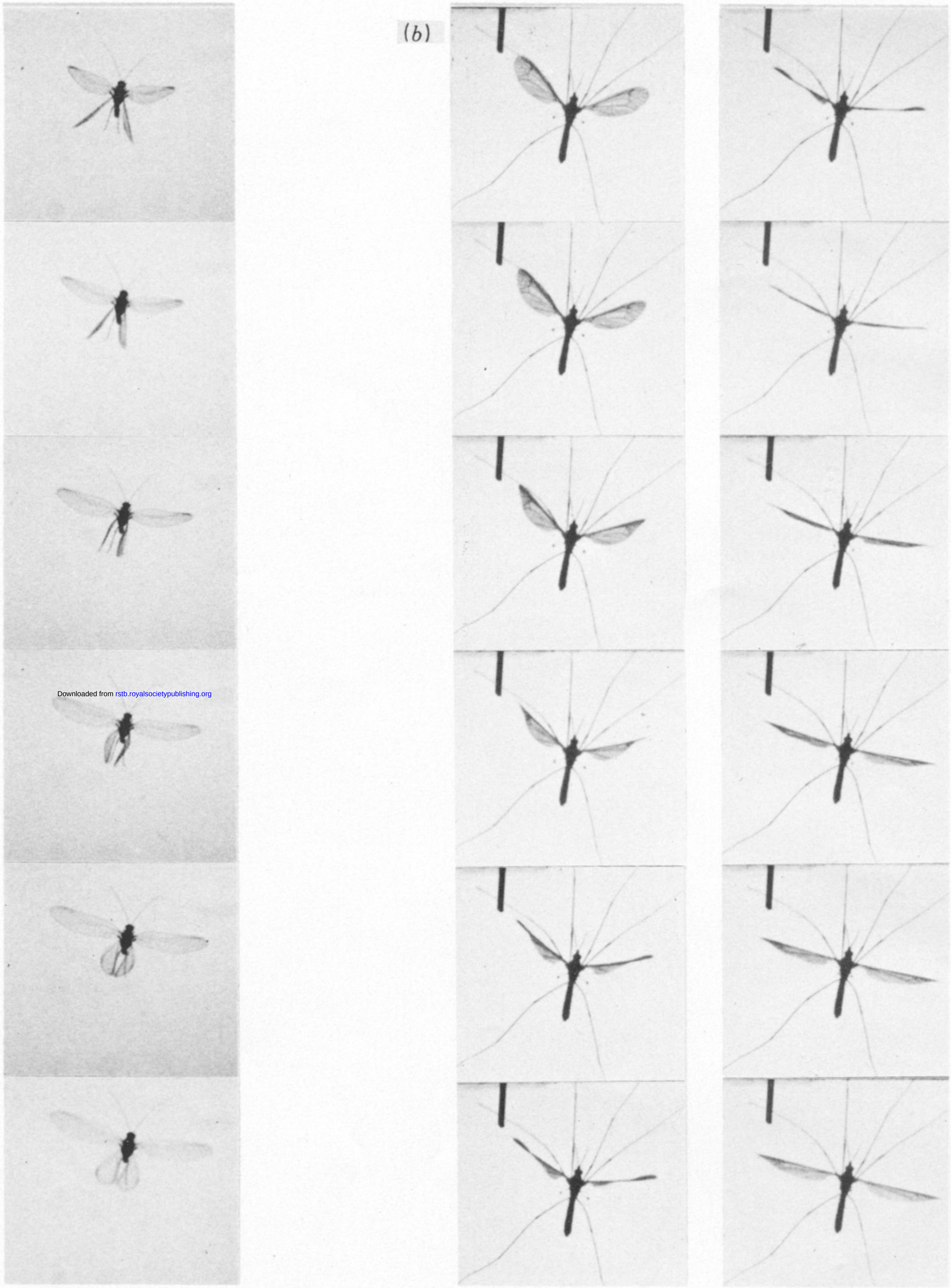

FIGURE 25. (*a*) A slight torsional wave moving towards the wing tip during supination of the hindwings of *Chrysopa*. (*b*) The latter half of supination for *Tipula obsoleta*. The anterior wing area rotates first, producing a torsional wave passing through the posterior region towards the wing base. Elastic recoil of the angle of attack is evident at the end of supination.